AD-A073 450 OKLAHOMA STATE UNIV STILLWATER FLUID POWER RESEARCH --ETC F/G 13/7
THE SURVIVABILITY CHARACTERISTICS OF FLUID POWER COMPONENTS IN --ETC(U)
JUN 78 N00014-75-C-1157

UNCLASSIFIED ONR-CR169-004-1 NL

1 OF 2
AD A073450

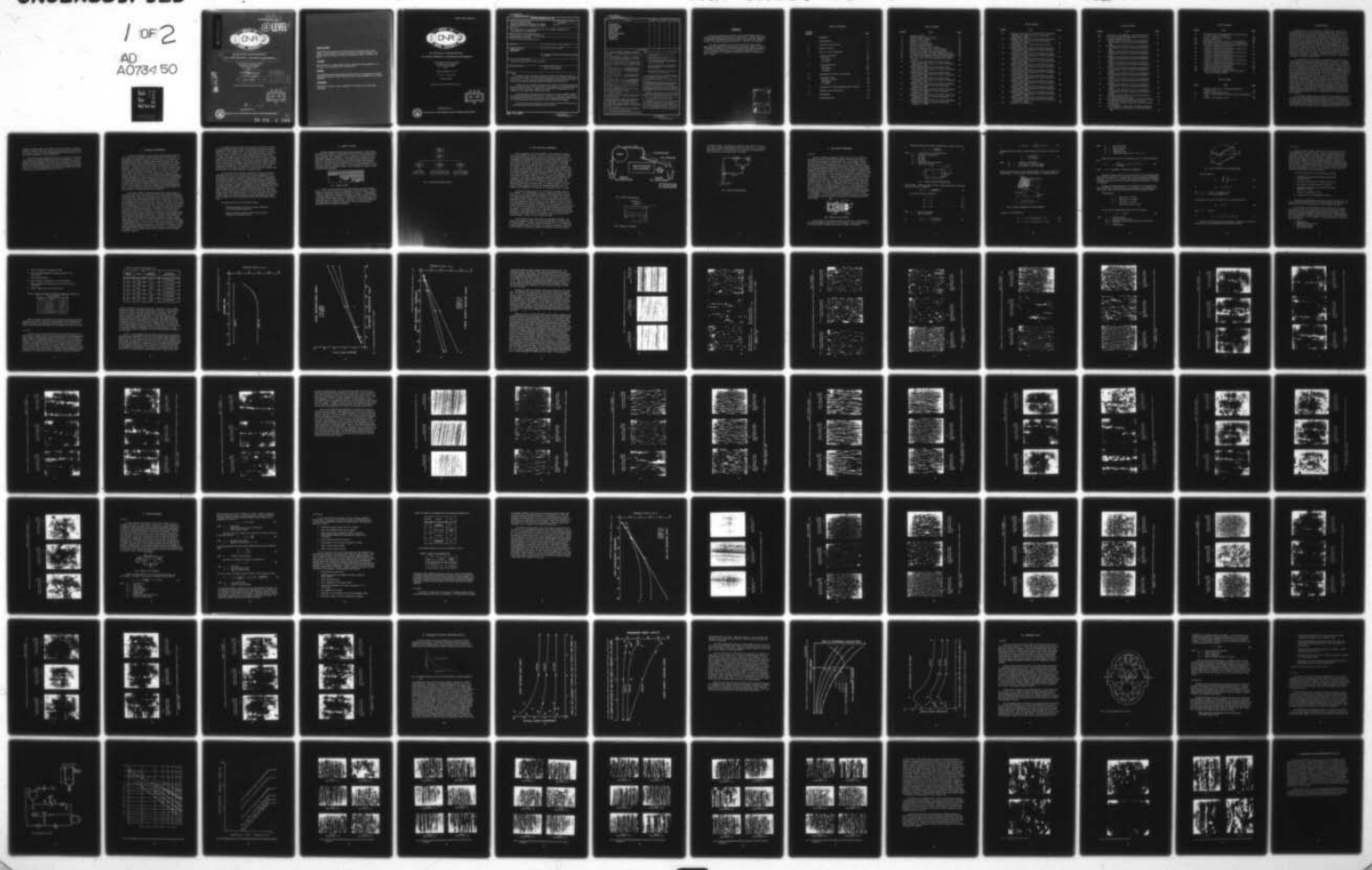

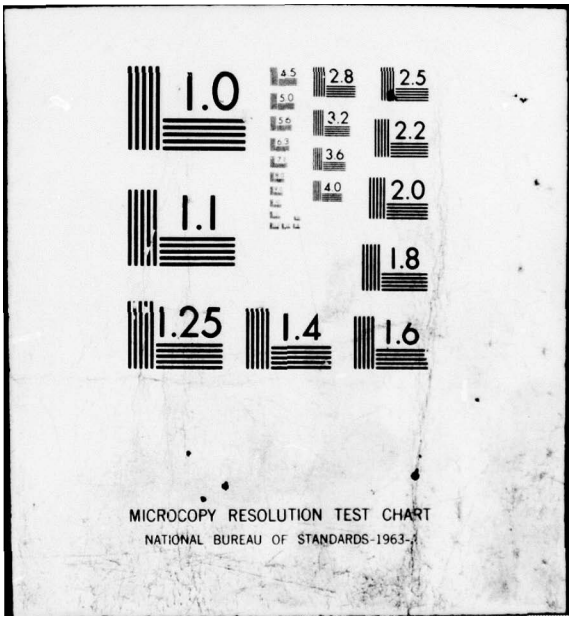
1.0
1.1
1.25
1.4
1.6
1.8
2.0
2.2
2.5
2.8
3.2
3.6
4.0
4.5
5.0
5.6
6.3
MICROCOPY RESOLUTION TEST CHART
NATIONAL BUREAU OF STANDARDS-1963-A

(18) (19)
REPORT ONR CR169-[illegible]-1

(12) LEVEL II

AD A045116

OFFICE OF NAVAL RESEARCH

(6) THE SURVIVABILITY CHARACTERISTICS OF
FLUID POWER COMPONENTS IN CONTAMINATED ENVIRONMENTS.

FLUID POWER RESEARCH CENTER
OKLAHOMA STATE UNIVERSITY
STILLWATER, OKLAHOMA
74074

(15) Contract No. N00014-75-C-1157

(12) 108p.

1 July 1977 – 30 June 1978

(9) ANNUAL REPORT. 1 Jul 77-30 Jun 78.

407 263

PREPARED FOR THE

OFFICE OF NAVAL RESEARCH ● 800 N. QUINCY ST. ● ARLINGTON ● VA ● 22217

bpg

Change of Address

Organizations receiving reports on the initial distribution list should confirm correct address. This list is located at the end of the report. Any change of address or distribution should be conveyed to the Office of Naval Research, Code 211, Arlington, VA 22217.

Disposition

When this report is no longer needed, it may be transmitted to other organizations. Do not return it to the originator or the monitoring office.

Disclaimer

The findings and conclusions contained in this report are not to be construed as an official Department of Defense or Military Department position unless so designated by other official documents.

Reproduction

REPORT ONR CR169–004–1

THE SURVIVABILITY CHARACTERISTICS OF FLUID POWER COMPONENTS IN CONTAMINATED ENVIRONMENTS

FLUID POWER RESEARCH CENTER
OKLAHOMA STATE UNIVERSITY
STILLWATER, OKLAHOMA
74074

Contract No. N00014–75–C–1157

1 July 1977 – 30 June 1978

ANNUAL REPORT

Approved for public release; distribution unlimited.

PREPARED FOR THE

OFFICE OF NAVAL RESEARCH ● 800 N. QUINCY ST. ● ARLINGTON ● VA ● 22217

UNCLASSIFIED
Security Classification

DOCUMENT CONTROL DATA - R&D
(Security classification of title, body of abstract and indexing annotation must be entered when the overall report is classified)

1. ORIGINATING ACTIVITY *(Corporate author)*
Fluid Power Research Center
Division of Engineering, Technology & Architecture
Oklahoma State University, Stillwater, OK 74074

2a. REPORT SECURITY CLASSIFICATION
Unclassified

2b. GROUP

3. REPORT TITLE
THE SURVIVABILITY CHARACTERISTICS OF FLUID POWER COMPONENTS IN CONTAMINATED ENVIRONMENTS

4. DESCRIPTIVE NOTES *(Type of report and inclusive dates)*
Annual Report – 1 July 1977 – 30 June 1978

5. AUTHOR(S) *(Last name, first name, initial)*
Staff of the Fluid Power Research Center

6. REPORT DATE	7a. TOTAL NO. OF PAGES	7b. NO. OF REFS

8a. CONTRACT OR GRANT NO.	9a. ORIGINATOR'S REPORT NUMBER(S)
N00014-75-C-1157 NR 169–004 b. PROJECT NO. c. d.	9b. OTHER REPORT NO(S) *(Any other numbers that may be assigned this report)*

10. AVAILABILITY/LIMITATION NOTICES
Approved for public release; distribution unlimited.

11. SUPPLEMENTARY NOTES	12. SPONSORING MILITARY ACTIVITY
	Office of Naval Research

13. ABSTRACT

Contaminant wear in fluid power components is a factor that limits the life and reliability of hydraulic systems. This wear normally takes place in areas of relative motion between two surfaces. In this study, tests were performed employing linear (reciprocating) and rotary motions to determine the relationship between contamination level and wear rate.

The tests reveal the importance of clearance size in relation to contaminant-induced wear. When the clearance between two moving surfaces is large compared to the contaminant size, the majority of wear will be erosive. However, as the contaminant size approaches that of the clearance, the wear mode shifts to include abrasive wear.

A component wear test conducted upon a hydraulic gear pump also revealed a relationship between contamination level and wear rate. In addition, it is shown that a correlation of pump wear data with the results of the linear and rotary rubbing wear tests provides an insight to the internal clearances of the pump and the resulting contaminant sensitivity.

The report covers the second phase of an ongoing effort to quantify the essential steps in maximizing system life versus contamination control investment.

DD FORM 1 JAN 64 1473

UNCLASSIFIED
Security Classification

14. KEY WORDS	LINK A		LINK B		LINK C	
	ROLE	WT	ROLE	WT	ROLE	WT
Contamination Contaminant Wear Critical Clearance Abrasive Wear Erosive Wear Hydraulic Components Wear Particles Ferrography Leakage Path						

INSTRUCTIONS

1. ORIGINATING ACTIVITY: Enter the name and address of the contractor, subcontractor, grantee, Department of Defense activity or other organization *(corporate author)* issuing the report.

2a. REPORT SECURITY CLASSIFICATION: Enter the overall security classification of the report. Indicate whether "Restricted Data" is included. Marking is to be in accordance with appropriate security regulations.

2b. GROUP: Automatic downgrading is specified in DoD Directive 5200.10 and Armed Forces Industrial Manual. Enter the group number. Also, when applicable, show that optional markings have been used for Group 3 and Group 4 as authorized.

3. REPORT TITLE: Enter the complete report title in all capital letters. Titles in all cases should be unclassified. If a meaningful title cannot be selected without classification, show title classification in all capitals in parenthesis immediately following the title.

4. DESCRIPTIVE NOTES: If appropriate, enter the type of report, e.g., interim, progress, summary, annual, or final. Give the inclusive dates when a specific reporting period is covered.

5. AUTHOR(S): Enter the name(s) of author(s) as shown on or in the report. Enter last name, first name, middle initial. If military, show rank and branch of service. The name of the principal author is an absolute minimum requirement.

6. REPORT DATE: Enter the date of the report as day, month, year, or month, year. If more than one date appears on the report, use date of publication.

7a. TOTAL NUMBER OF PAGES: The total page count should follow normal pagination procedures, i.e., enter the number of pages containing information.

7b. NUMBER OF REFERENCES: Enter the total number of references cited in the report.

8a. CONTRACT OR GRANT NUMBER: If appropriate, enter the applicable number of the contract or grant under which the report was written.

8b, 8c, & 8d. PROJECT NUMBER: Enter the appropriate military department identification, such as project number, subproject number, system numbers, task number, etc.

9a. ORIGINATOR'S REPORT NUMBER(S): Enter the official report number by which the document will be identified and controlled by the originating activity. This number must be unique to this report.

9b. OTHER REPORT NUMBER(S): If the report has been assigned any other report numbers *(either by the originator or by the sponsor)*, also enter this number(s).

10. AVAILABILITY/LIMITATION NOTICES: Enter any limitations on further dissemination of the report, other than those imposed by security classification, using standard statements such as:

(1) "Qualified requesters may obtain copies of this report from DDC."

(2) "Foreign announcement and dissemination of this report by DDC is not authorized."

(3) "U. S. Government agencies may obtain copies of this report directly from DDC. Other qualified DDC users shall request through _____."

(4) "U. S. military agencies may obtain copies of this report directly from DDC. Other qualified users shall request through _____."

(5) "All distribution of this report is controlled. Qualified DDC users shall request through _____."

If the report has been furnished to the Office of Technical Services, Department of Commerce, for sale to the public, indicate this fact and enter the price, if known.

11. SUPPLEMENTARY NOTES: Use for additional explanatory notes.

12. SPONSORING MILITARY ACTIVITY: Enter the name of the departmental project office or laboratory sponsoring *(paying for)* the research and development. Include address.

13. ABSTRACT: Enter an abstract giving a brief and factual summary of the document indicative of the report, even though it may also appear elsewhere in the body of the technical report. If additional space is required, a continuation sheet shall be attached.

It is highly desirable that the abstract of classified reports be unclassified. Each paragraph of the abstract shall end with an indication of the military security classification of the information in the paragraph, represented as *(TS), (S), (C), or (U)*.

There is no limitation on the length of the abstract. However, the suggested length is from 150 to 225 words.

14. KEY WORDS: Key words are technically meaningful terms or short phrases that characterize a report and may be used as index entries for cataloging the report. Key words must be selected so that no security classification is required. Identifiers, such as equipment model designation, trade name, military project code name, geographic location, may be used as key words but will be followed by an indication of technical context. The assignment of links, rules, and weights is optional.

FOREWORD

This report was prepared by the staff of the Fluid Power Research Center at Oklahoma State University of Agriculture and Applied Science. The study was initiated by the Office of Naval Research at Arlington, Virginia, under Contract No. N00014–75–C–1157. The time period covered by this report is 1 July 1977 – 30 June 1978.

This study was effectively monitored by Commander Kirk Petrovic, whose guidance and participation contributed significantly to the overall success of the effort. The program was conducted at the Fluid Power Research Center under the direction of Dr. R. K. Tessmann, Program Manager, with guidance and consultation from Dr. E. C. Fitch, Center Director. Dr. Tessmann was ably assisted by Mr. D. E. Kitzmiller and Mr. R. J. Smith.

TABLE OF CONTENTS

LIST OF FIGURES

LIST OF FIGURES

LIST OF FIGURES

LIST OF FIGURES

LIST OF TABLES

I. INTRODUCTION

Contaminant wear can be the single most influential factor limiting hydraulic component service life. In an effort to control contaminant wear, millions of dollars are spent annually for filters of all kinds, replacement parts, components, and the maintenance associated with these items. Inexorably, the thought of *"If some filtration is good, then more must be better."* has produced a trend toward finer and finer degrees of filtration to control contaminant wear. Without a doubt, filtration is necessary; however, some consideration must be given to the trade-offs involved. What is the point of maximum return on the contamination control investment? It must be recognized that filtration costs money. Not only the initial expenditure but also in the costs required to maintain the filtration level. These costs are not fixed; for example, a filter which exhibits a filtration ratio at 10 μM of 10 may cost more than an equally sized $\beta_{10} = 2$ filter and also may have less dirt capacity and a higher pressure drop (which adds an energy cost to the total). It seems quite possible then that there is an optimum level of filtration, a point where the service life of a system is maximized with full regard to the filtration investment made.

This report covers the second phase of an ongoing effort to quantify essential steps in maximizing system life versus contamination control investment. The objective of these phases was to establish the relationship between component life and its environmental contamination level. The obvious method to attack such a problem would be a series of varying contamination level tests on hydraulic components. However, this would result in an unending series of testing, since the simplest of design differences from component to component (even among the same type) could result in significant changes in the contaminant sensitivity of the components. The method utilized in this effort avoids that by attacking the problem at a basic level. That is: all components are systems (assemblages of parts that together form a synergistic entity). The contaminant wear occurring in these assemblies or components takes place most significantly in areas of relative motion between two parts of the component. Further, there are two kinds of motion which make up the majority of actions found in these components, a rotary rubbing action (such as exists between a gear and a wear plate or a pump valve block and the casing) and a linear rubbing action (normally reciprocating) as typified by a hydraulic cylinder or a sliding spool valve. Therefore, determination of the relationship between contamination level and wear rate in these simple mechanisms will provide important information regarding the effect of contamination level on assemblies of these basic mechanisms.

The Fluid Power Research Center has assembled two model mechanisms for study, one rotary and one linear (reciprocating) along with the necessary support equipment. The basic systems have already been in use as described in Ref. [1]. This report covers the second year of study which consists of the results from the continuing effort on the basic mechanisms and the results of the first component tests (gear pumps) in the program. The first year's effort was devoted entirely to mechanisms and the results of the first

component tests (gear pumps) in the program. The first year's effort was devoted entirely to a mechanism wear study, and the results from that portion of the program will be used in this report to further establish correlation between contaminant wear and various test parameters of the basic mechanisms.

Test results have been evaluated by use of the new technology of Ferrography. This technique of wear analysis presents data that other methods cannot, in that it provides for efficient separation of wear debris from a fluid sample. The debris thus separated is permanently retained and may be evaluated both objectively and subjectively for information regarding its origin, type, and severity of the wear mode which produced it. A further understanding of the mechanics of Ferrography and its potential in fluid power may be gained from Refs. [2, 3, 4, 5].

II. TECHNICAL BACKGROUND

In a normally functioning fluid power system, filtration elements operate in such a manner so as to establish a relatively constant fluid contamination level. The more effective the filtration, the lower the contamination level. The system fluid, intended among other things to lubricate system components, paradoxically carries contaminant particles to wear susceptible surfaces in each component. The resulting rate of wear is some function of the contaminant concentration and particle size distribution. If these two factors could be reduced to an infinitely small level, great reductions in contaminant wear could be achieved. The *"infinite"* service life which might intuitively be expected from operation in such a *"super clean"* environment will, in reality, never occur due to wear from other sources. However, since contaminant wear is such a large factor in the service life of most hydraulic components, significant improvement in component service life would stem from increased filtration (i.e., reduced contamination) levels. The objectives of this phase of the project are to provide information regarding the relationship between fluid contamination level and wear in basic hydraulic mechanisms and begin to apply that knowledge toward the study of wear reduction in fluid power components by decreasing contamination levels. In order to effectively interpret data from these series of tests, however, the basic phenomena of the wearing process must be understood.

The two main categories of contaminant-induced wear are erosive wear and abrasive (three-body) wear. Erosive wear is the result of free particles impinging upon the wearing surface. Bitter [6, 7] attributes the erosive wearing action to deformation of the material under repeated particle collisions and to a cutting action on the material by contaminant particles. Although potentially a source of severe wear, erosion is normally overshadowed by three-body abrasive wear. Abrasive wear is similar in some respects to erosive cutting wear, since it is also the result of particles cutting or plowing material from a surface; however, the motive force in this case is no longer simply the particle's own momentum (and fluid viscous forces). In three-body wear, the cutting force is provided by a second surface in relative motion to the first. This type of wear is evident when clearances are small enough to trap contaminant particles between surfaces with enough force to produce the cutting action. Khruschov [8, 9] established precedence for abrasive wear studies when he utilized a mechanism consisting of abrasive coated paper in relative motion to a metallic specimen under unlubricated conditions. Other investigators [10, 11, 12, 13, 14, 15] followed his lead, but not until this decade was significant work done in the area of wear in fluid power components. For example, in 1972, noteworthy progress was made with the introduction of the Bensch and Fitch Contaminant Sensitivity Theory for Fluid Power Pumps [16]. In the last three years, other papers [17, 18, 19] have provided important concepts concerning component contaminant sensitivity.

The contaminant sensitivity theory, even though a great stride in the direction of true contamination control, still relies on measurements of performance parameter degradation to reflect component wear. It does not present any method to directly measure wear in the component nor to relate performance degradation to surface wear. This was a definite *"stumbling block"* in the universal application of these efforts. The advent of Ferrography as a wear analysis technique has surmounted the problem by providing the means to measure the amount of wear debris in a system to a greater degree of accuracy than ever before. Other methods of wear debris analysis have been utilized in the past, the most notable of these being spectroscopy. While the spectrometer has been applied to fluid power systems analysis, it has not enjoyed widespread acceptance in this application. The Ferrograph is well suited to its task of wear debris analysis in fluid systems, particularly in the case of contaminant accelerated wear, and has proved to be a viable complement to spectroscopy [20].

In an actual fluid power component, abrasive wear is normally the dominant contaminant wear mode. In the first phase of this study, as reported by Ref. [1], the situations of two surfaces in rotational relative motion and linear relative motion were simulated by separate mechanisms. To determine the effect of a contaminated environment on these two types of mechanisms, particulate contaminant (AC Fine Test Dust, ACFTD) was introduced into the fluid being circulated through the mechanisms. The tests were arranged to evaluate the mechanisms's wear at various concentrations and size ranges of contaminant particles. This provided for a broad application of the results, since contaminant concentration and particle size distribution may vary widely from system to system dependent on its filtration and external environment. The constant factor of the first phase of effort was the fact that all tests were conducted at a single clearance, which is not normally the case in a *"real world"* component. Even with this condition, however, the results were promising, as they indicated significant improvements in component life could be possible by decreasing contaminant levels of system fluids.

The second phase of effort has been directed toward:

1. **broadening the application of the first year's results by repeating those tests at a different (smaller) clearance, and**

2. **beginning the program of component testing to provide the necessary correlation with the mechanism test data.**

III. SCOPE OF EFFORT

The report considers the second phase, which was intended to provide information regarding the relationship of contamination level and fluid power component survivability. The overall effort (as illustrated in Fig. 1) began with a critical examination of contaminant wear in basic mechanisms. A basic rotary motion mechanism and a basic linear motion mechanism were evaluated. The rationale for such a beginning may be seen from an examination of Fig. 2, which reveals the contaminant wear parameter hierarchy. It should be noted that attempting to vary all of these parameters would result in an extremely involved test program. The fact that each component in a system may present many wear situations (as shown in Fig. 2) indicates the complexity of the contaminant wear phenomenon.

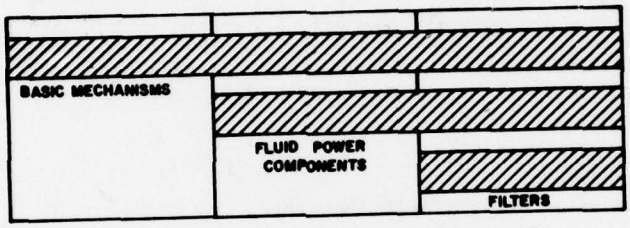

Fig. 1. Complete Test PGM.

In Fig. 1, it may be seen that Phase I dealt exclusively with basic mechanism studies. In that effort, three of the nine parameters of Fig. 2 were varied. They were contaminant concentration, particle size distribution, and material. The second phase of effort, as reported here, expands that knowledge by a change in a fourth dimension – clearance between the two surfaces. In all other respects, the mechanism tests of the second phase followed those of the first. Additionally, the second year extended into contaminant wear of a system component – gear pumps. An extensive pump test program was successfully completed with variations in two of the basic parameters – contaminant size and contaminant concentration.

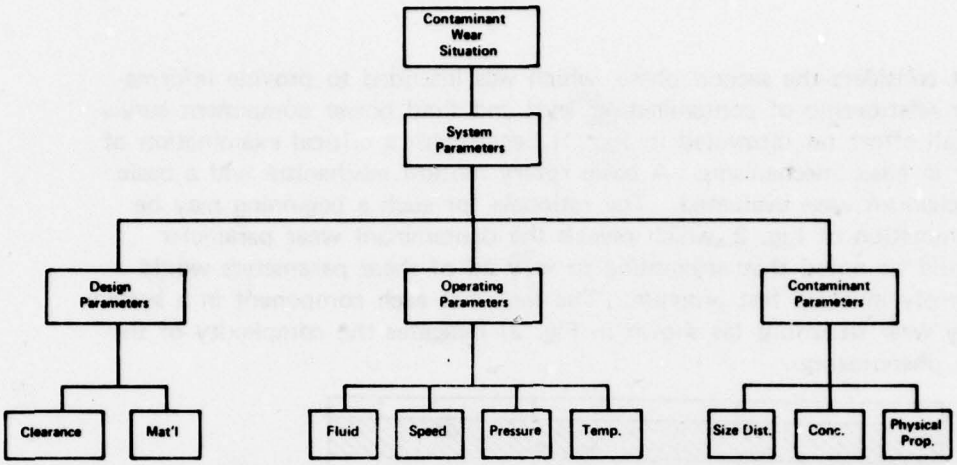

Fig. 2. Contaminant Wear Parameter Hierarchy.

IV. DATA ANALYSIS TECHNIQUES

Of key importance in any scientific endeavor are the methods and equipment used in data acquisition and analysis. In order for a study such as this to be successful, data analysis techniques must give results in an accurate and unbiased manner. The necessity for a high degree of confidence normally indicates reliance on more than one method of data analysis. In other words, an engineer involved in complicated research should not rely on a single data source for his conclusions. In this study, two methods of data analysis have been utilized – one primary and one secondary. In all cases (i.e., rotary mechanism tests, linear mechanism tests, and component tests), the primary analysis technique is Ferrography. As a secondary analysis technique used for comparative purposes, a performance parameter change was monitored. In the case of the linear mechanism, this parameter was leakage; in the rotary mechanism, a dimensional change in the wearing surfaces; and, for the gear pumps, flow degradation. While not used as a prime indicator, these performance parameters provided real-time trend indications and were logical parallel parameters to the Ferrographic analysis. The primary analysis was made on a Duplex Ferrograph Analyzer in conjunction with a Bichromatic Microscope and Ferrogram Reader. A complete description of the Ferrographic Technique, equipment, operation, and characteristics was given in Ref. [1]. However, a brief explanation of the workings of the Ferrographic System is in order.

The Duplex Ferrograph, shown in Fig. 3, produces the Ferrograms which are to be analyzed. This is accomplished by pumping a predetermined sample volume of system fluid across a specially treated glass substrate. The substrate rests in the field of a powerful permanent magnet in such a manner that the magnetic field strength increases along the slide. Particles present in the sample respond to several forces as the fluid moves longitudinally down the substrate, the most important of which are magnetic, viscous, gravitational, and mechanical (interference). For ferrous particles, the most influential of these forces is caused by the magnetic field; a large majority of those particles are *"captured"* by the magnetic field. Particles with weaker magnetic properties exhibit less response to the magnetic field and are, in some cases, carried completely across the substrate into a waste bottle along with the oil itself. A *"fixer"* solution is passed across the substrate, which washes it free of any remaining oil film, and the substrate (now called a Ferrogram, as shown in Fig. 4) is labeled and stored.

The first process is only an interim step in the Ferrographic Technique. The analysis is accomplished by means of the Bichromatic Microscope in conjunction with the Ferrogram Reader. The system is shown schematically in Fig. 5. The densitometer (Ferrogram Reader) measures the disturbance of a light beam by particles. The amount of light reflected by the particles is measured and presented on the digital readout of

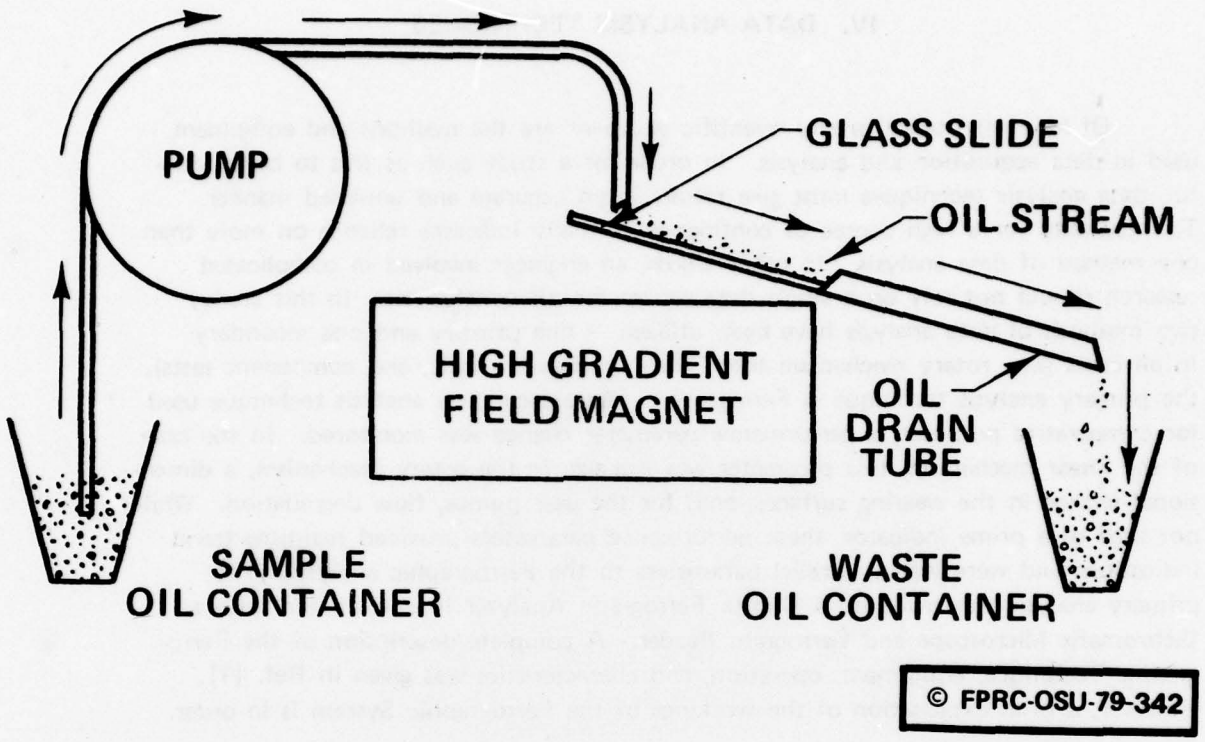

Fig. 3. Schematic of Slide Ferrograph.

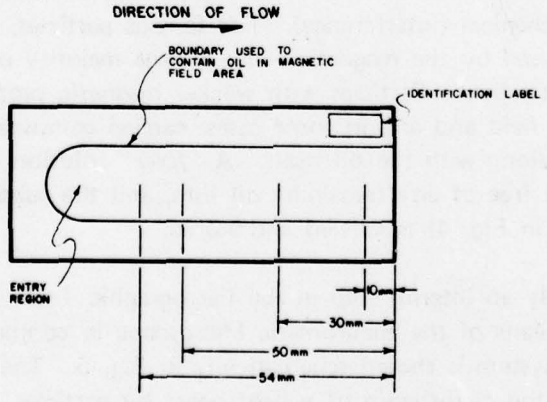

Fig. 4. Illustration of a Ferrogram.

the Ferrogram Reader. The Ferrograph in particular is well suited to this type of study, since it ignores extraneous particles (the AC Fine Test Dust) in measuring the wear debris particles. It is this separation of wear debris from unwanted particles which is the key to the Ferrograph's value in hydraulics.

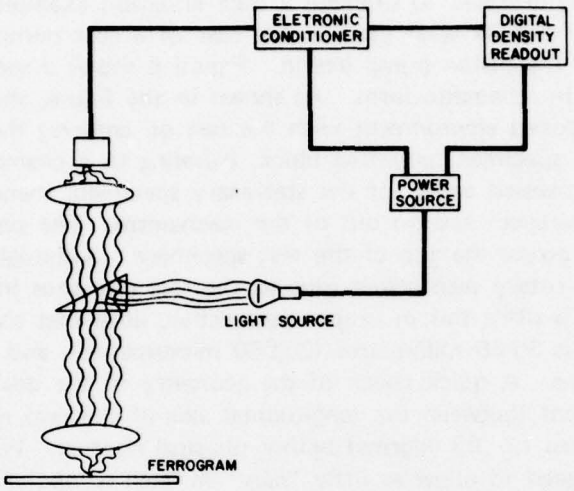

Fig. 5. Schematic of Ferrogram Reader.

V. THE ROTARY MECHANISM

Description

The rotary mechanism is designed to simulate a wear situation exemplified by such cases as the side of a gear and its wear plate in the case of a gear pump or a valve block and pump body in the piston pump design. Figure 6 shows a sectional view of the rotary mechanism in schematic form. As shown in the figure, the test specimens function in an oil-flooded environment with the test oil entering the mechanism through the stationary test specimen mounting block, traveling to a chamber formed by the rotating specimen and recessed center of the stationary specimen, thence escaping through the radial gap (test clearance) and on out of the mechanism. The pressure drop noted in the test conditions is across the gap of the test specimens. Although of a simple and straightforward design, the rotary mechanism (due to the test clearance involved) is an extremely precise device. To place this in proper perspective, note that the stationary test specimen's outer diameter is 35.56 millimetres (35,560 micrometres), and the test clearance is only 10 micrometres. A quick check of the geometry of the device shows an allowable angular misalignment (between the longitudinal axis of the two test specimens) of only 5.6×10^{-4} radians ($\approx$ .03 degrees) before physical contact. With this in mind, the mechanism was designed to allow as little *"play"* in each component as possible. The ball bearings were widely spaced and a preload nut incorporated into the mechanism to reduce any misalignment. The stationary side of the mechanism consists of a 63.5 millimetre diameter spool, 101.6 millimetres long with a nominal clearance of 12.7 micrometres. This restricts the maximum misalignment to 1.25×10^{-4} radians ($\approx$ .007 degrees). In order to provide as exact an alignment as possible, the two halves of the mechanism casing were provided with alignment and locking screws around the mating flanges.

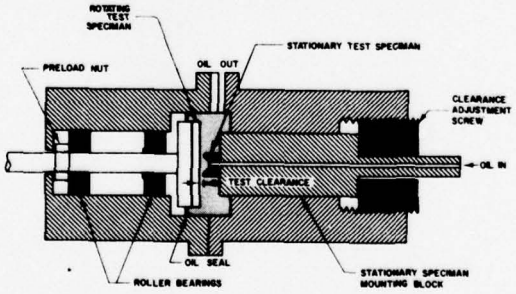

Fig. 6. Schematic of Rotary Mechanism.

The importance of the mechanism alignment may be seen in an examination of the theoretical equations of flow through the test clearance. Figure 7 depicts the situation of flow through a rectangular gap of width, w; length, l; and height, h.

Pressure-induced fluid flow through a rectangular gap is modeled by Ref. [2] as:

$$Q = k_1 \frac{\Delta P\ w\ h^3}{\mu\ l} \tag{1}$$

where:
- Q = volume flow due to pressure differential
- k_1 = constant for rectangular gap
- w = gap width
- h = gap height
- l = gap length
- ΔP = pressure differential across length
- μ = fluid dynamic viscosity

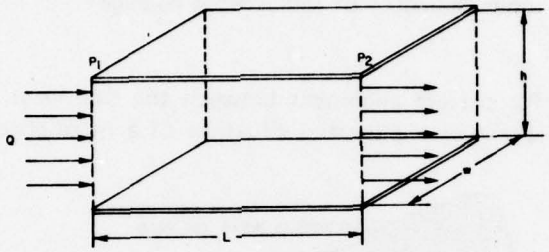

Fig. 7. Fluid Flow Through a Rectangular Passage.

A gap of height, h, differential length, dl, width, dw, and pressure drop, dp, and differential flow, dQ, may be modeled as:

$$dQ\ dl = k_1 \frac{dP\ dw\ h^3}{\mu} \tag{2}$$

In the case of the rotary mechanism,

$$h = h \tag{3}$$

$$dP = dP \tag{4}$$

$$dl = dr \tag{5}$$

$$dw = r d\phi \tag{6}$$

where:
- r = radius of flow passage
- ϕ = angle from reference

So:

$$dQ\ dr = \frac{k_1\ h^3\ dP\ r d\phi}{\mu} \tag{7}$$

or:

$$\frac{1}{r}\, dQ\, dr = \frac{k_1\, h^3}{\mu}\, dP\, d\phi \qquad (8)$$

Integrating Eq. (8) with suitable boundary conditions and solving for volume flow, Q, gives:

$$Q = \frac{k_2\, \pi\, \Delta P\, h^3}{\mu \ln (R/R_o)} \qquad (9)$$

where:
- k_2 = constant for radial passage
- R = outer diameter of radial flow passage
- R_o = inner diameter of radial flow passage

Equation (9) is valid only for perfect alignment between the two wear surfaces in the rotary mechanism. Figure 8 shows a potential situation of a misaligned mechanism.

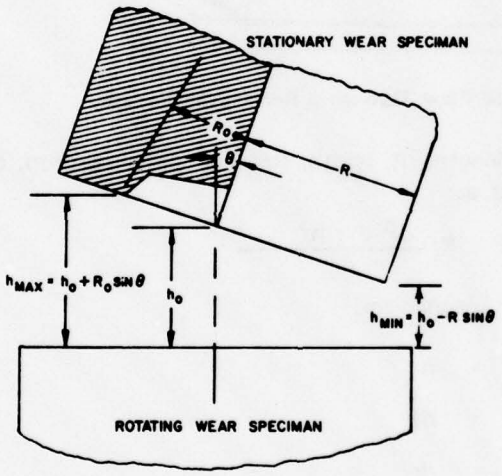

Fig. 8. Illustration of Misalignment in the Rotary Mechanism.

The gap, h, is now expressed as:

$$h_1 = h_o + R_o \sin\theta \sin\phi \quad \{o \leq \phi < \pi\} \qquad (10)$$

$$h_2 = h_o + R \sin\theta \sin\phi \quad \{\pi \leq \phi < 2\pi\} \qquad (11)$$

where: h_o = gap at center line
h_1 = gap on *"high"* side
h_2 = gap on low side
θ = misalignment angle
ϕ = angle in plane of gap from ϕ = o @ $h_1 = h_2$

Inserting Eqs. (10) and (11) into the differential form of Eq. (9) and integrating gives:

$$Q_p = k_3 \frac{\Delta P}{\mu \ln (R/Ro)} [h_o^3 + k_4 R^2 \theta^2 h_o] \quad (12)$$

where: k_3, k_4 = constants for radial gap with misalignment

Equation (12) points out that flow is a strong function of the misalignment angle. Under the physical parameters of this mechanism, the flow increases (as the misalignment goes from $\theta = 0$ to $\theta = \theta_{max}$) by 120%! Test personnel took advantage of this sensitivity to precisely align each specimen prior to testing by observing flow response to θ changes in all directions.

Although an interesting derivation, Eq. (12) represents only the stationary case. When the plates are in relative motion, the rotating plate acts as a centrifugal pump to alter the flow. Figure 9 shows the stresses on the fluid during mechanism rotation.

These stresses are:

τ_r = viscous shear in r direction
τ_θ = viscous shear in w direction
a_r = acceleration in r direction
w = relative rotary velocity of plates

In Ref. [22], the resulting radial velocity of the fluid is given as:

$$V_r = rw\, f(\delta) \quad (13)$$

where: V_r = radial fluid velocity
r = distance from axis of rotation
$f(\delta)$ = dimensionless radial velocity distribution as a function of Z
δ = Z (w/ν)
ν = kinetic viscosity

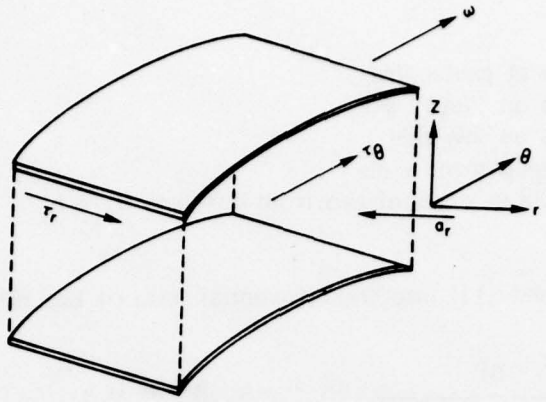

Fig. 9. Stresses on Fluid Between Plates in Relative Rotation.

The flow therefore is:

$$Q_c = \int_0^{2\pi} \int_0^{h} v_r \, dz \, r \, d\theta \tag{14}$$

or

$$Q_c = k_4 \, f(R^2, w, h) \tag{15}$$

where: Q_c = flow due to centrifugal pumping
k_4 = constant for centrifugal flow

The total flow is the sum of the pressure flow, Q, and centrifugal flow, Q_c:

$$Q_t = Q_c + Q \tag{16}$$

where: Q_t = total flow

or:

$$Q_t = f(\rho, R, R_o, \theta, \mu, \Delta P, h, w) \tag{17}$$

Equation (17) illustrates the important parameters of these tests. The reader will note that all of the above parameters were held constant throughout.

Test Procedure

Tests of the rotary mechanism consisted of a five step sequence of events: fabricate, assemble, align, break-in, and test. Fabrication entailed lapping both the rotating disk and wear specimen until local variations in height of the wearing surfaces were minimized. After a careful cleaning of the lapping compound from the pieces, they were installed in the rotary mechanism. Alignment was a two fold process, first the rotating disk and then the stationary specimen. Alignment of the disk was with the reference to the center line of rotation, and adjustment was normally not necessary. The stationary wear specimen was fastened to its mounting block, which was then installed in the housing, as shown in Fig. 6. Alignment of the wear specimen was accomplished by means of the three adjustment screws located 120° around the mating flanges of the two housing halves.

The break-in procedure for each new specimen was as follows:

1. **Circulate filtered oil through mechanism without rotating until test temperature is reached.**
2. **Adjust clearance and bypass valve for 50 psid and .04 l/min. flow.**
3. **Run mechanism for 15 minutes. Sample at end of period.**
4. **Adjust clearance and bypass valve to increase pressure by 50 psid, keeping flow at .04 l/min.**
5. **Repeat 3 and 4 until 400 psid is reached.**
6. **At 400 psid, run for one hour, sampling every 15 minutes.**

This procedure circulated filtered oil through the rotating mechanism for 2 3/4 hours at clearances ranging from 20 down to 10 micrometres (the test clearance). This procedure was carried out for each new wear specimen utilized in the tests.

The test procedure itself was designed to allow measurement of the effect of varying contaminant sizes and concentrations on the wear rate of the test specimen. These were the only two parameters varied throughout the individual tests. Table I shows other important test parameters which were held constant. These constant parameter values are identical to those of mechanism tests in the first phase of this effort with the exception of h – the test clearance. The test procedure for the rotary mechanism was as follows:

1. **Break-in specimen.**
2. **Establish test conditions per Table I.**
3. **Switch filters out of system.**
4. **Extract background sample.**

5. Inject 0-5 μM ACFTD at a concentration of 5 mg/l.

6. Run for 14 minutes, maintaining test conditions, and sample at 2, 4, 8, and 14 minutes.

7. Filter system for 30 minutes.

8. Repeat 3 through 7 for concentrations of 10, 20, 40, and 80 mg/l.

9. Repeat 1 through 8 for contaminant sizes of 0-30 and 0-80 μM using new wear specimen.

10. Repeat 1 through 9 for each wear specimen material.

TABLE I. Summary of Test Parameter Held Constant During Rotary Mechanism Tests.

Constant Test Parameters		
Symbol	Description	Value
Δp	Pressure Drop	27.6 bars
ω	Rotating Velocity	1550 rpm
T	Fluid Temperature	38°C
h	Test Clearance	10 μm
Q	Flow Through Mechanism	.04 ℓ/min

Table II delineates the various contamination/material combinations which were subjected to this procedure. Note that a new wear specimen was used with each contaminant size range. The contaminant sizes were selected in order to provide (with respect to the clearance) one size smaller, one size somewhat larger, and one size larger.

Test Results

The effect of the various contaminant sizes and concentrations utilized in this series of tests is presented in the form of graphs plotting these two factors against Ferrographic densities. The Ferrographic data are the optical density at the 43 millimetre location (recall this is termed D54) divided by the volume of oil utilized in making the Ferrogram. This normalization allows Ferrograms which differ greatly in their amount of debris to be compared on a common basis. The Ferrographic densities reflect the amount of metallic debris contained in the Ferrogram sample. Metal in the sample is a result of wear occurring in the mechanism. Therefore, the density readings are a direct indicator of wear. The oil samples used for Ferrographic analysis contained wear debris accumulated in the system fluid over the time span beginning with the contaminant

TABLE II. Summary of Rotary Mechanism Tests.

Specimen Number	Material	Contaminant Size Range (μm)	Contaminant Concentrations (mg/ℓ)
A-1	Alum.	0-5	5, 10, 20, 40, 80
A-2	Alum.	0-30	5, 10, 20, 40, 80
A-3	Alum.	0-80	5, 10, 20, 40, 80
B-1	Brass	0-5	5, 10, 20, 40, 80
B-2	Brass	0-30	5, 10, 20, 40, 80
B-3	Brass	0-80	5, 10, 20, 40, 80

injection and ending at that particular sample time. Consequently, a plot of D54/ml versus time should be a curve with a slope indicative of wear rate. During the initial minutes of an injection, wear sample densities plot as a straight line. After a short period of time, however, the wear rate rapidly slows and approaches zero. This is probably the result of contaminant destruction. In these rotary mechanism tests, continual adjustment maintains a constant clearance, and careful design prevents contaminants from settling or being filtered out during tests. The decrease in wear rate is exemplified by Fig. 10, which shows typical Ferrographic density in terms of D54/ml readings plotted against time from the rotary mechanism tests. Since the accumulation of wear stabilizes after some initial period, any sample taken in the latter portion of the injection should be representative of the wear which has occurred. In order to insure that the samples are representative, the last (14 minute) sample was chosen for use in this study.

In Fig. 11, the Ferrographic density readings are plotted against the contaminant concentration (in milligrams/litre) for the rotary test mechanism with the brass/steel wear specimen installed. Three traces are shown for the 0-5, 0-30, and 0-80 micrometre contaminant sizes. The same information is given in Fig. 12 for the rotary mechanism using aluminum/steel wear specimens. It may be seen that the two figures are almost identical, although the aluminum/steel data indicated more wear at the larger particle size range. It is also apparent that the wear occurring in these tests is a function of contaminant size and contarninant concentration. In both figures, the concentration seems to have a greater effect on the wear process than does contaminant size. Note that, when the

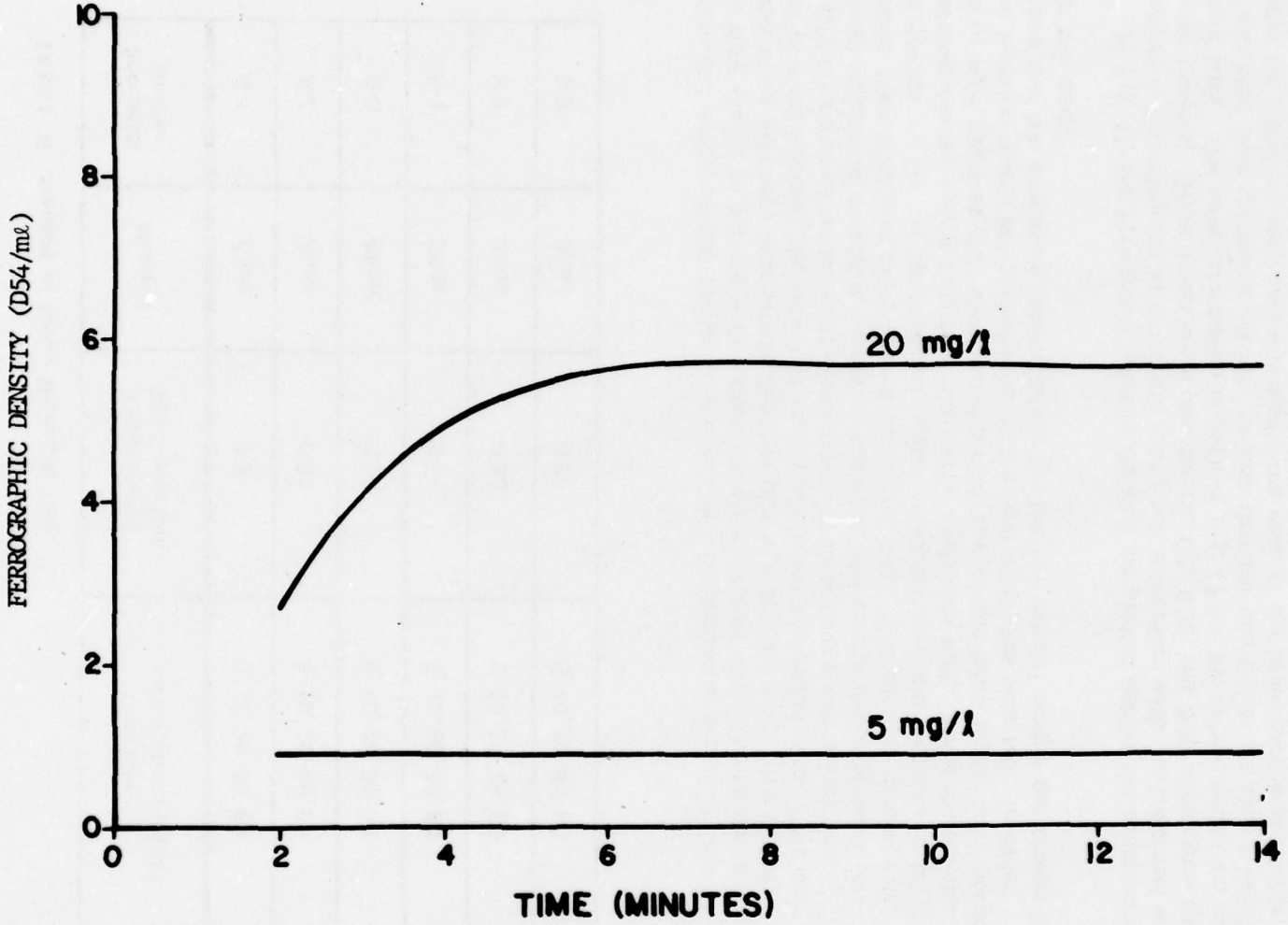

Fig. 10. Typical Rotary Mechanism Ferrographic Densities versus Time.

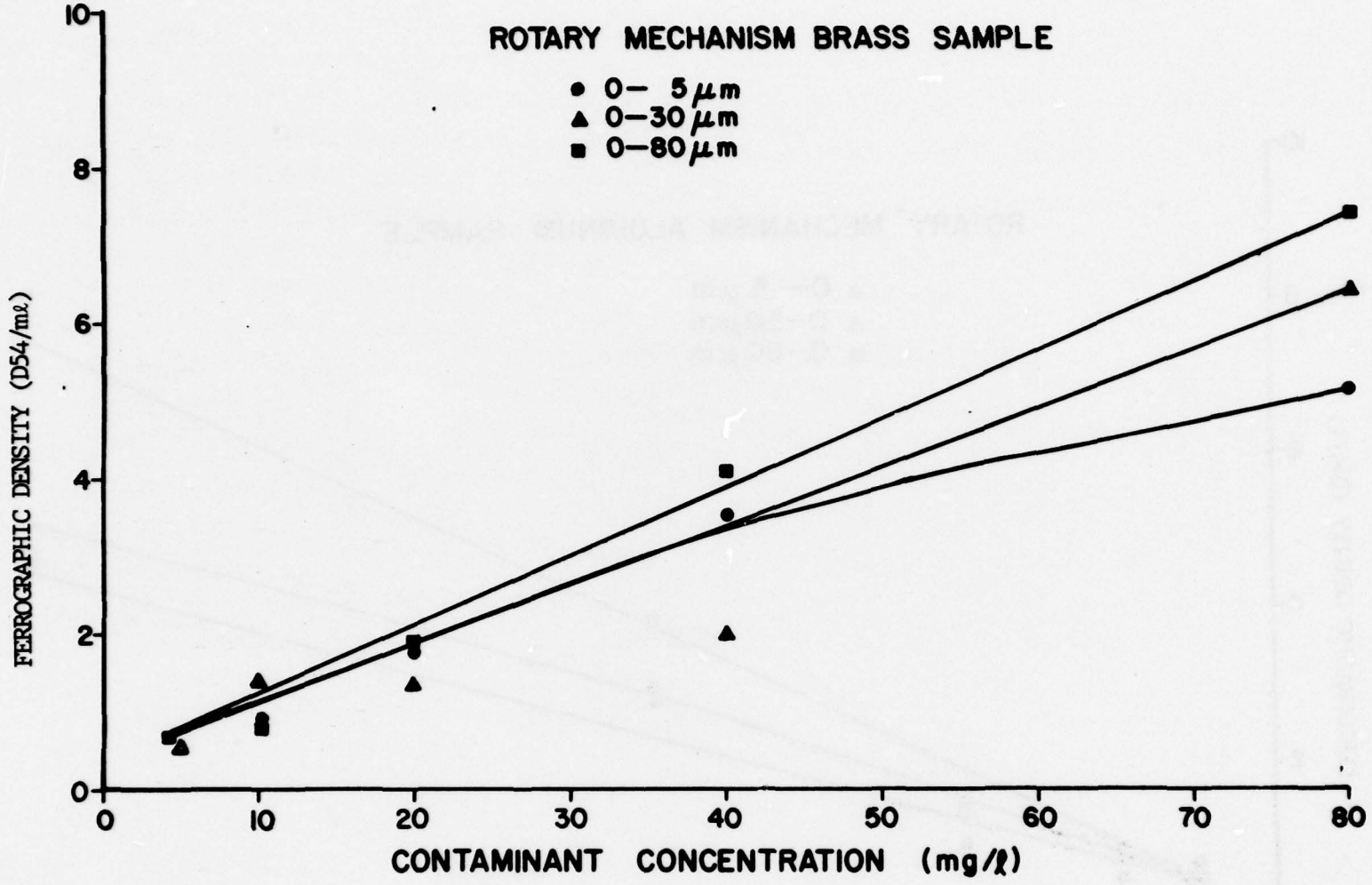

Fig. 11. Test Results, Rotary Mechanism with Brass/Steel Wear Specimen.

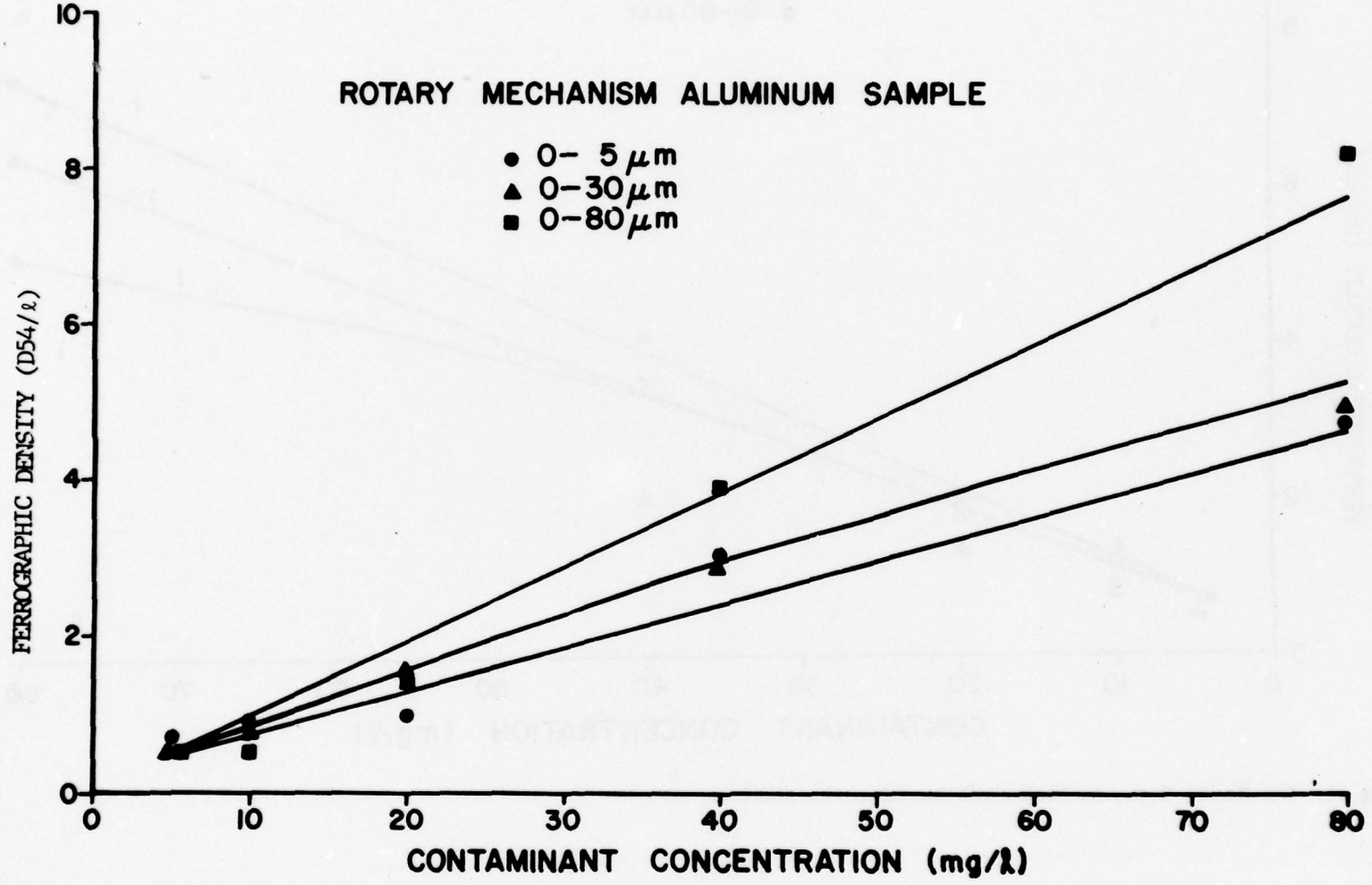

Fig. 12. Test Results, Rotary Mechanism with Aluminum-Steel Specimen.

concentration doubles, the density readings in each case essentially double. (The implication of greatly reduced rates of wear with reducing contamination levels is particularly significant in this project, since a primary objective is increased component life through reduced contamination levels.) The influence of particle size range can also be observed in these figures. Here, the wear rate is shown to be a direct function of contaminant size (that is, wear increases as size increases), but the relationship is not 1:1. That is, the wear rate observed during the 0-80 micrometre injection is not 16 times greater than the wear rate of the 0-5 micrometre contaminant. Similarly, the 0-30 micrometre curve's relationship to those of the other two does not reflect the ratio of the sizes.

Although it is, many times, difficult to garner useful information from a photograph, the appearance of the wearing surface is of sufficient interest to be presented here. In Fig. 13, the three photos show the surfaces of the brass specimen after each had been exposed to all contaminant concentrations used in the rotary tests. The first (left-hand) picture is of the brass surface after exposure to 0-5 micrometre test dust. The magnification in all cases is 50X. In this first photo, the orientation is such that the center of rotation of the specimen is directly below the photo, with the direction rotation of the specimen being from right to left. The picture shows how the test contaminant traveled outward in a tight spiraling path, gouging out material as it went. The remaining two photos depict much the same information in addition to showing the difference in *"surface finish"* resulting from the 0-30 and 0-80 micrometre contaminant sizes.

Figures 14, 15, 16, 17, and 18 were made at the 54 millimetre location on the Ferrograms prepared from the 14-minute sample. These are the same Ferrograms which provided the data for the preceding graphs. In each figure, the concentration remains the same for all three photos, but the contaminant size will vary, the left-hand photo being of debris from a 0-5 micrometre contaminant injection sample, the center a 0-30 micrometre injection sample, and the right-hand a 0-80 micrometre injection sample. Magnification in each case is 100X. The photographs taken across the page depict the effects of increasing contaminant size, following in another direction; that is, from figure to figure, each photo (of debris from 0-5 micrometre contaminant injection) illustrates the effects on increasing contaminant concentration. Note that varying amounts of sample oil were used to prepare these Ferrograms; and, to attempt to compare the amount of material on one picture to another without taking this factor into account could lead to an incorrect conclusion. With this in mind, no comments regarding the absolute amount of material present will be made. In Fig. 14, it is apparent that the sample was drawn from the tests utilizing a brass wear specimen. A number of brassy colored particles can be seen to be larger and not as ordered as the ferrous material. As a general guide, it can be assumed that all dark particles which have collected in the vertical strands are ferrous wear debris. Figure 15 provides much the same information as Fig. 14. Figures 16, 17, and 18 serve to further illustrate typical Ferrogram appearance. The next set of photographs which comprise Figs. 19-23 repeat Figs. 14-18, however, at a higher magnification of 1000X (rather than 100X). This is sufficient to

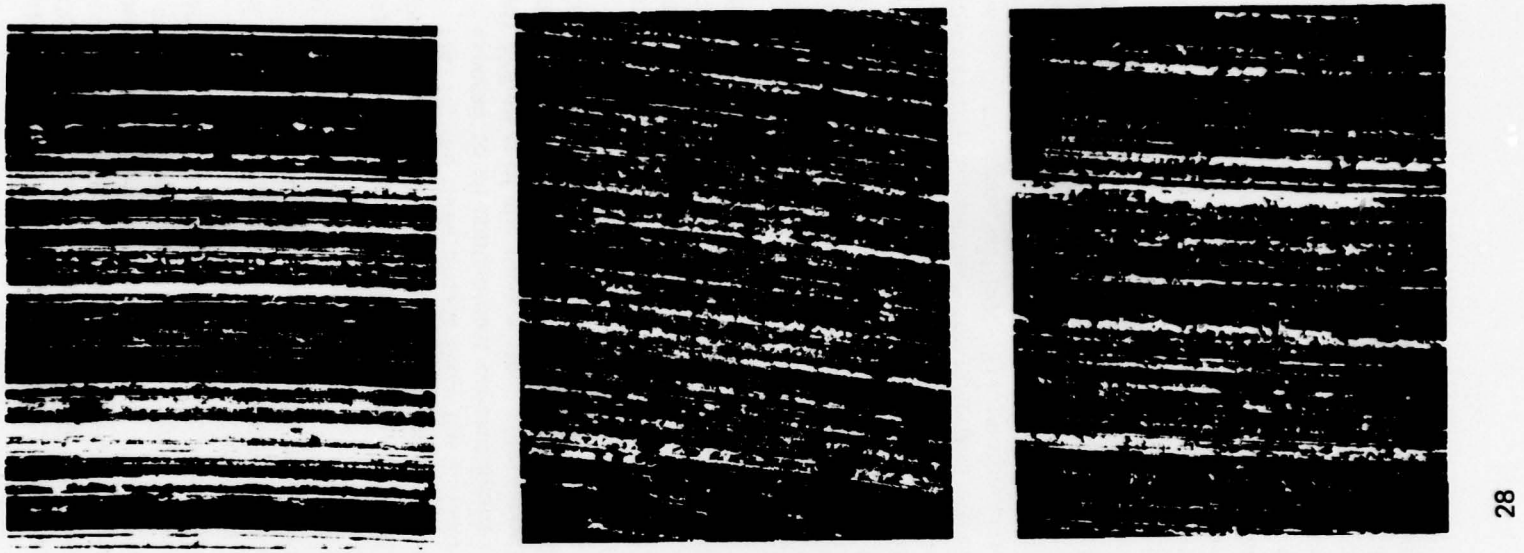

(a)

After Exposure to 0-5 μM
Particle Size Range

(b)

After Exposure to 0-30 μM
Particle Size Range

(c)

After Exposure to 0-80 μM
Particle Size Range

Fig. 13. Brass Test Specimen from Rotary Mechanism After Indicated Exposure (Magnification = 50X).

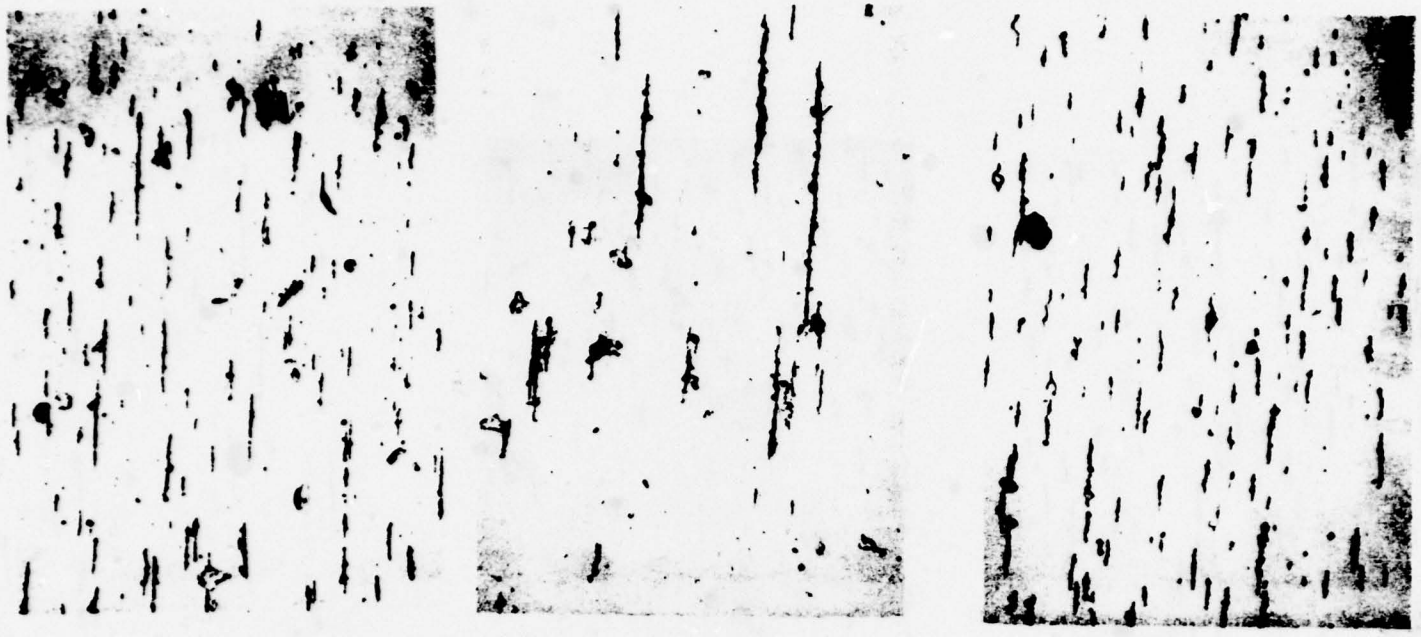

(a) After Exposure to 0-5 μM Particle Size Range (Volume = 12 ml)

(b) After Exposure to 0-30 μM Particle Size Range (Volume = 12 ml)

(c) After Exposure to 0-80 μM Farticle Size Range (Volume = 12 ml)

Fig. 14. Ferrograms of Wear Debris (54 mm) from Brass on Steel Rotary Mechanism after Exposure to 5 mg/litre (Magnification = 100X).

(a)

After Exposure to 0-5 μM
Particle Size Range (Volume = 12 ml)

(b)

After Exposure to 0-30 μM
Particle Size Range (Volume = 12 ml)

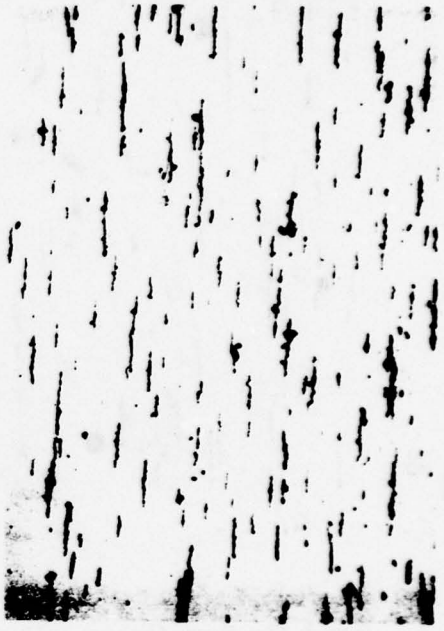

(c)

After Exposure to 0-80 μM
Particle Size Range (Volume = 12 ml)

30

Fig. 15. Ferrograms of Wear Debris (54 mm) from Brass on Steel Rotary Mechanism after Exposure to 10 mg/litre of Contaminant (Magnification = 100X).

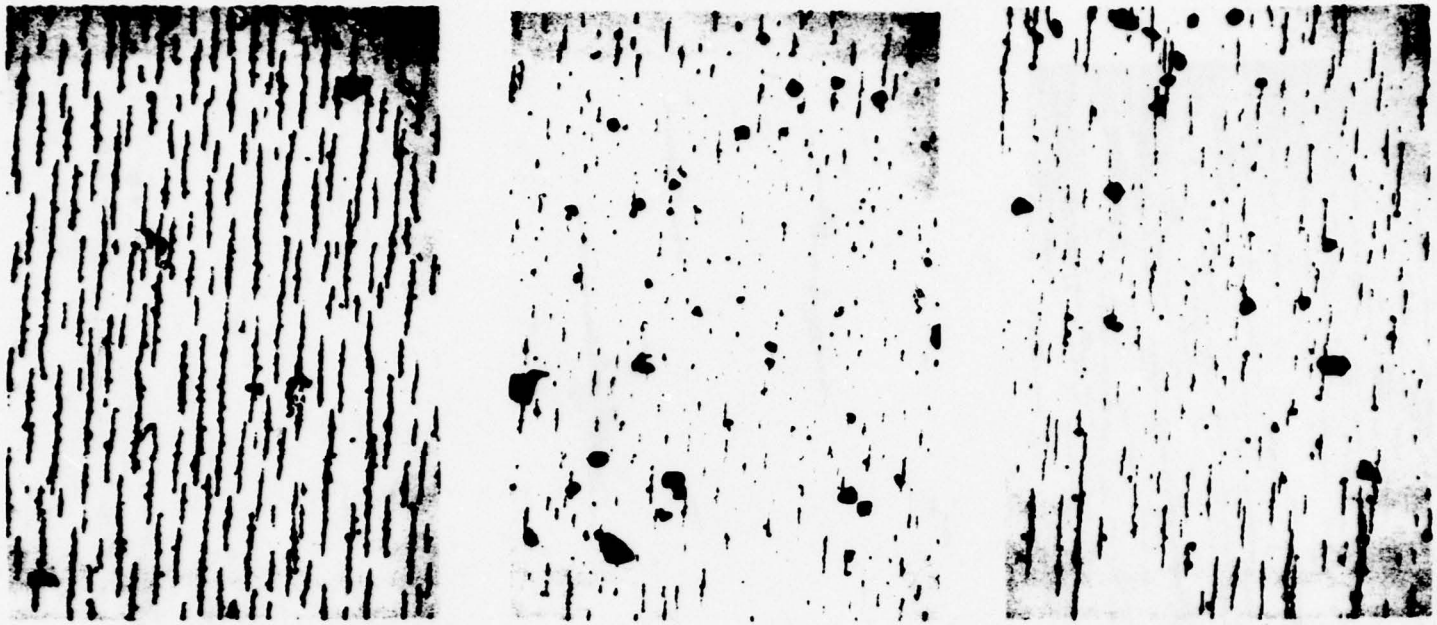

(a)

After Exposure to 0-5 μM Particle Size Range (Volume = 12 ml)

(b)

After Exposure to 0-30 μM Particle Size Range (Volume = 6 ml)

(c)

After Exposure to 0-80 μM Particle Size Range (Volume = 6 ml)

Fig. 16. Ferrograms of Wear Debris (54 mm) from Brass on Steel Rotary Mechanism After Exposure to 20 mg/litre of Contaminant (Magnification = 100X).

(a)

After Exposure to 0-5 μM Particle Size Range (Volume = 6 ml)

(b)

After Exposure to 0-30 μM Particle Size Range (Volume = 6 ml)

(c)

After Exposure to 0-80 μM Particle Size Range (Volume = 3 ml)

Fig. 17. Ferrograms of Wear Debris (54 mm) from Brass on Steel Rotary Mechanism after Exposure to 40 mg/litre of Contaminant (Magnification = 100X).

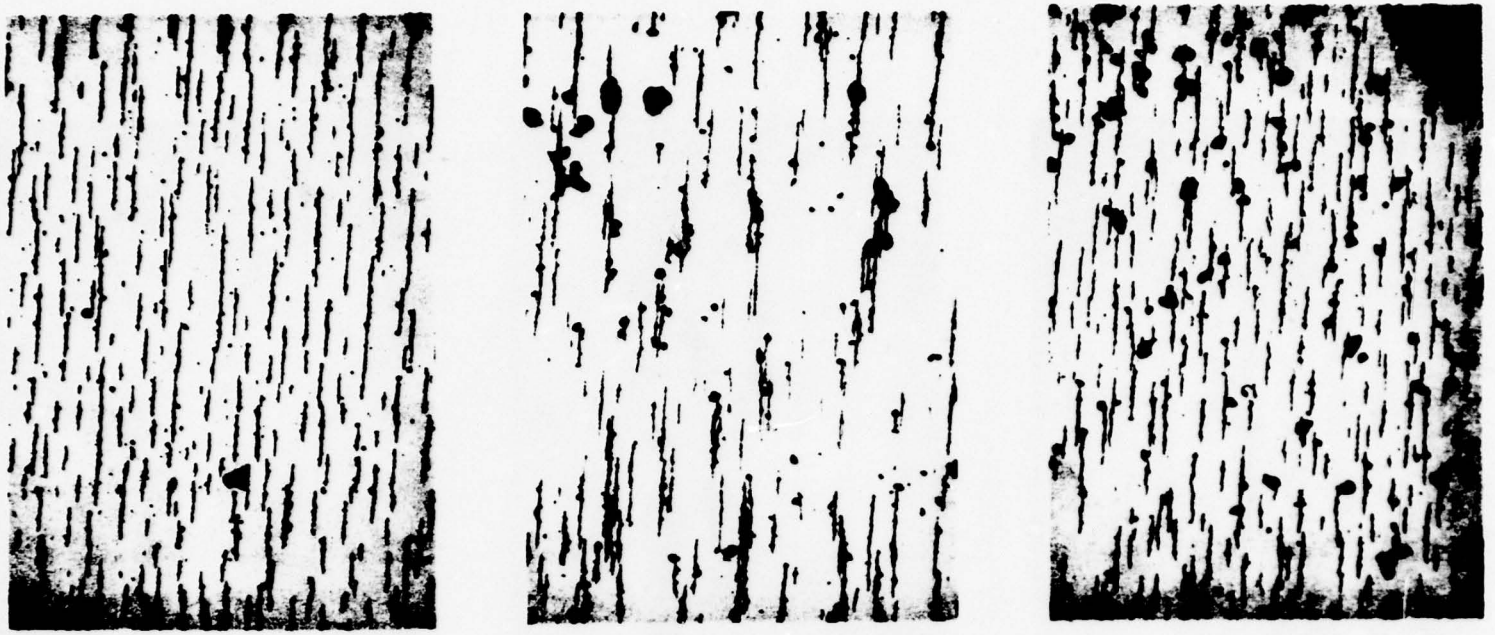

(a)

After Exposure to 0-5 μM Particle Size Range (Volume = 3 ml)

(b)

After Exposure to 0-30 μM Particle Size Range (Volume = 3 ml)

(c)

After Exposure to 0-80 μM Particle Size Range (Volume = 3 ml)

Fig. 18. Ferrograms of Wear Debris (54 mm) from Brass on Steel Rotary Mechanism after Exposure to 80 mg/litre of Contaminant (Magnification = 100X).

(a)

After Exposure to 0-5 μM Particle Size Range (Volume = 12 ml)

(b)

After Exposure to 0-30 μM Particle Size Range (Volume = 12 ml)

(c)

After Exposure to 0-80 μM Particle Size Range (Volume = 12 ml)

Fig. 19. Ferrograms of Wear Debris (54 mm) from Brass on Steel Rotary Mechanism after Exposure to 5 mg/litre of Contaminant (Magnification = 1000X).

(a)

After Exposure to 0-5 μM Particle Size Range (Volume = 12 ml)

(b)

After Exposure to 0-30 μM Particle Size Range (Volume = 12 ml)

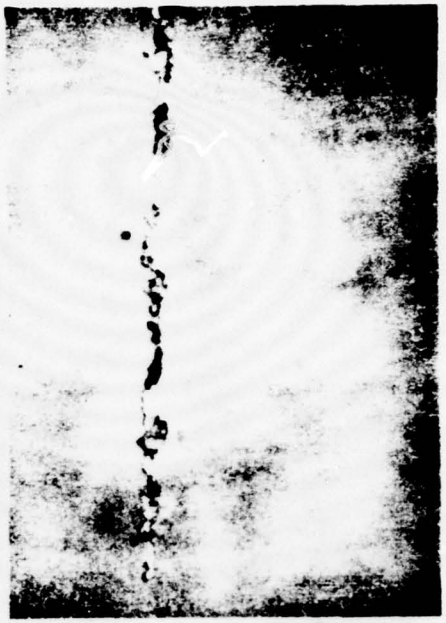

(c)

After Exposure to 0-80 μM Particle Size Range (Volume = 12 ml)

Fig. 20. Ferrograms of Wear Debris (54 mm) from Brass on Steel Rotary Mechanism after Exposure to 10 mg/litre of Contaminant (Magnification = 1000X).

(a)

After Exposure to 0-5 μM Particle Size Range (Volume = 12 ml)

(b)

After Exposure to 0-30 μM Particle Size Range (Volume = 6 ml)

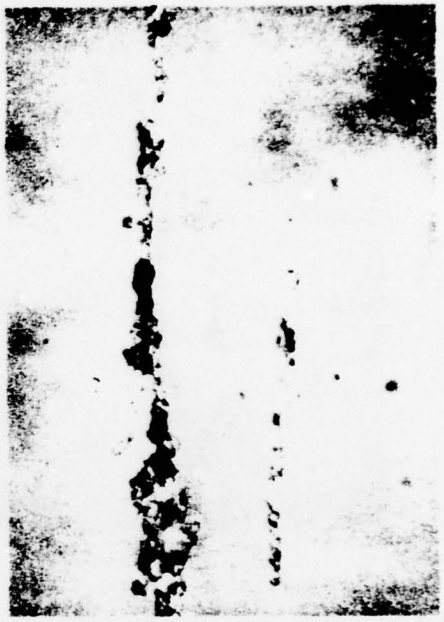

(c)

After Exposure to 0-80 μM Particle Size Range (Volume = 6 ml)

Fig. 21. Ferrograms of Wear Debris (54 mm) from Brass on Steel Rotary Mechanism after Exposure to 20 mg/litre of Contaminant (Magnification = 1000X).

(a)

After Exposure to 0-5 μM Particle Size Range (Volume = 6 ml)

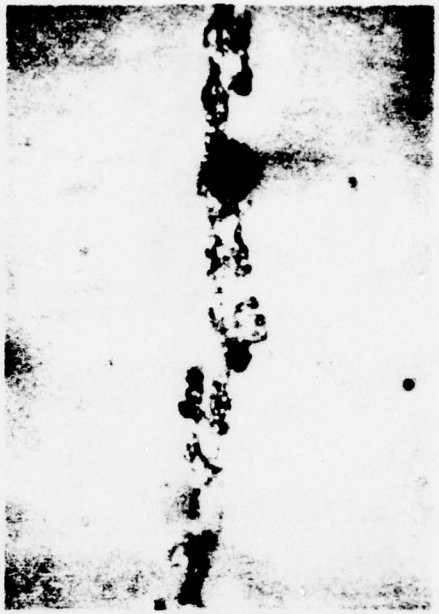

(b)

After Exposure to 0-30 μM Particle Size Range (Volume = 6 ml)

(c)

After Exposure to 0-80 μM Particle Size Range (Volume = 3 ml)

Fig. 22. Ferrograms of Wear Debris (54 mm) from Brass on Steel Rotary Mechanism After Exposure to 40 mg/litre of Contaminant (Magnification = 1000X).

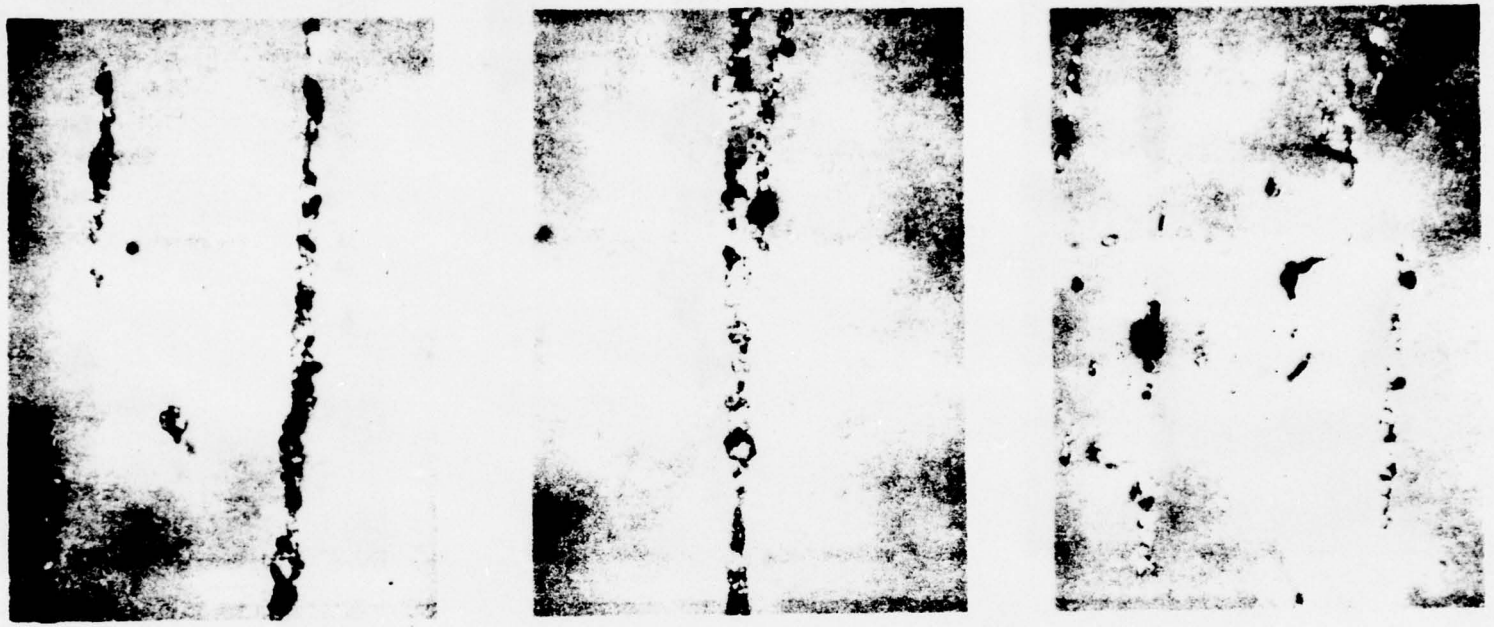

(a)

After Exposure to 0-5 μM Particle Size Range (Volume = 3 ml)

(b)

After Exposure to 0-30 μM Particle Size Range (Volume = 3 ml)

(c)

After Exposure to 0-80 μM Particle Size Range (Volume = 3 ml)

Fig. 23. Ferrograms of Wear Debris (54 mm) from Brass on Steel Rotary Mechanism after Exposure to 80 mg/litre of Contaminant (Magnification = 1000X).

distinguish individual particles in most cases, and even the casual observer may note the lathe chip-like wear particles, normally termed cutting wear. This three-body wear mode would be expected to occur only when the contaminant included particles much larger than the test clearance. Therefore, the absence of cutting wear in the 0-5 micrometre photographs, the few cutting wear particles in the 0-30 micrometre injection photographs, and the many cutting wear particles in the 0-80 micrometre pictures should come as no surprise. In addition, the field of view in each photograph is approximately 50 x 75 micrometres. Therefore, while every attempt was made to provide photos of particles which were representative of the region, there is naturally some variation.

Figure 24, Figs. 25-29, and Figs. 30-34 depict the surface of the three rotary mechanism aluminum samples – 100X magnifications of the 54 millimetre location of each 14-minute sample Ferrogram and 1000X magnifications of the same 54 millimetre locations, respectively. Since the information is much the same as the preceding group of figures, accompanying remarks will be brief. In Fig. 24, the direction of rotation is again right to left; however, in this case, particularly in the photograph of the 0-5 micrometre contaminant debris, scoring in a direction other than parallel to the motion is evident. Figures 25-29 appear much the same as the 100X photographs from the rotary brass/steel test. Conspicuously absent, however, is any evident aluminum debris (which should show as large bright particles). This could be due to the differing magnetic properties of brass and aluminum or from differences in the wear occurring on the (brass or aluminum) specimen itself. The high magnification (1000X) photographs of Figs. 30-34 again allow observation of the individual wear debris particles; and, again, cutting wear particles may be noted in many of the photos of debris from 0-30 and 0-80 micrometre contaminant injections.

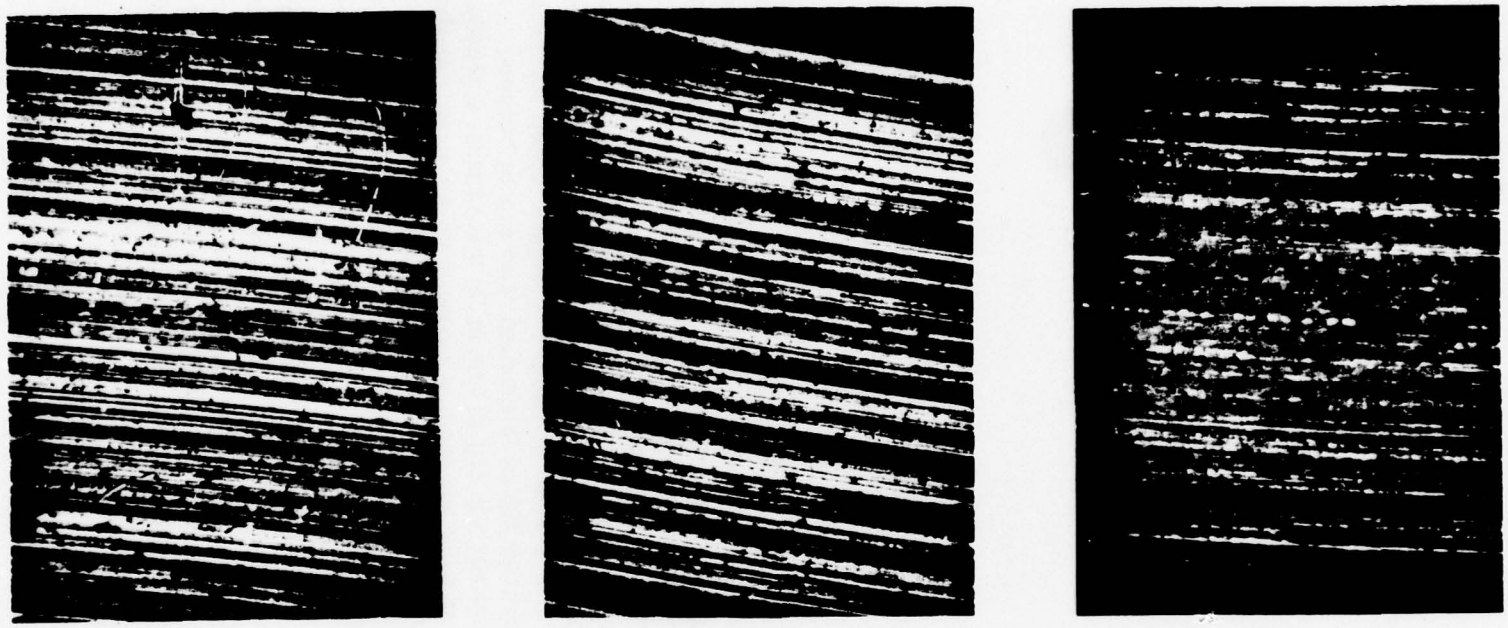

(a)

After Exposure to 0-5 μM
Particle Size Range

(b)

After Exposure to 0-30 μM
Particle Size Range

(c)

After Exposure to 0-80 μM
Particle Size Range

Fig. 24. Aluminum Specimen After Indicated Contaminant Exposure (Magnification = 50X).

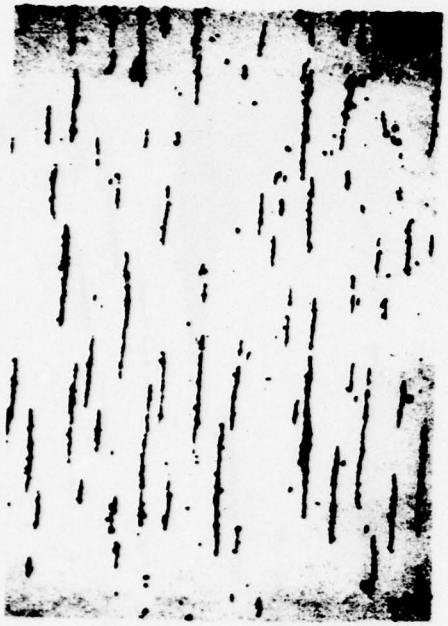

(a)

After Exposure to 0-5 μM Particle Size Range (Volume = 12 ml)

(b)

After Exposure to 0-30 μM Particle Size Range (Volume = 12 ml)

(c)

After Exposure to 0-80 μM Particle Size Range (Volume = 12 ml)

Fig. 25. Ferrograms of Wear Debris (54 mm) from Aluminum on Steel Rotary Mechanism after Exposure to 5 mg/litre of Contaminant (Magnification = 100X).

(a)

After Exposure to 0-5 μM Particle Size Range (Volume = 12 ml)

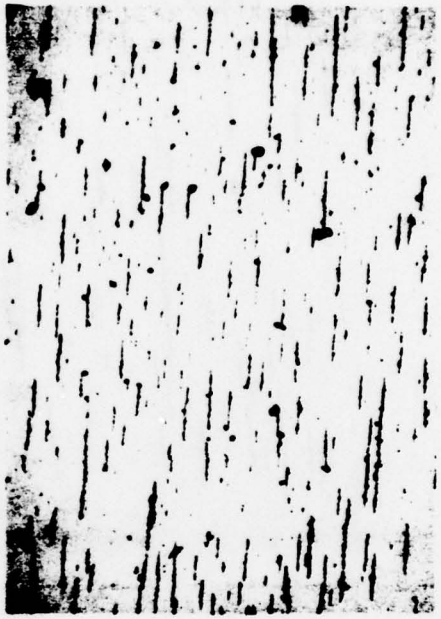

(b)

After Exposure to 0-30 μM Particle Size Range (Volume = 12 ml)

(c)

After Exposure to 0-80 μM Particle Size Range (Volume = 12 ml)

Fig. 26. Ferrograms of Wear Debris (54 mm) from Aluminum on Steel Rotary Mechanism After Exposure to 10 mg/litre of Contaminant (Magnification = 100X).

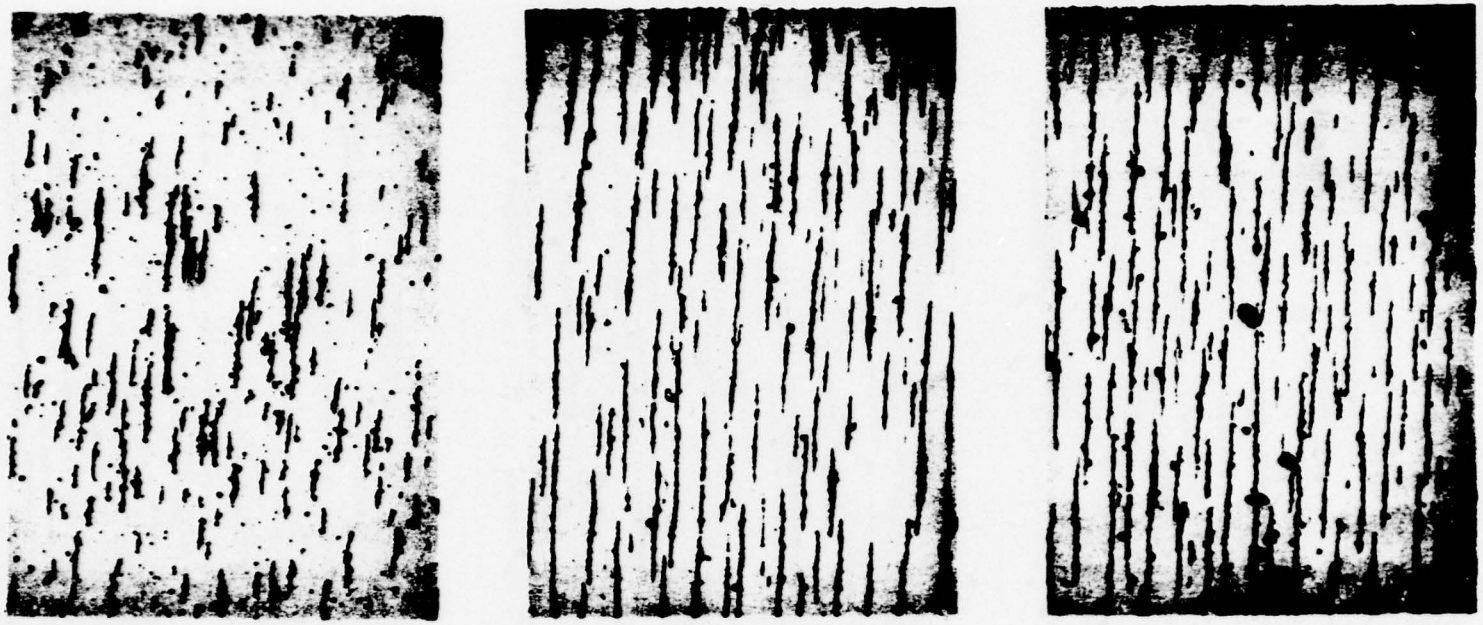

(a)

After Exposure to 0-5 μM Particle Size Range (Volume = 12 ml)

(b)

After Exposure to 0-30 μM Particle Size Range (Volume = 12 ml)

(c)

After Exposure to 0-80 μM Particle Size Range (Volume = 12 ml)

Fig. 27. Ferrograms of Wear Debris (54 mm) from Aluminum on Steel Rotary Mechanism After Exposure to 20 mg/litre of Contaminant (Magnification = 200X).

(a)

After Exposure to 0-5 μM Particle Size Range (Volume = 6 ml)

(b)

After Exposure to 0-30 μM Particle Size Range (Volume = 6 ml)

(c)

After Exposure to 0-80 μM Particle Size Range (Volume = 6 ml)

Fig. 28. Ferrograms of Wear Debris (54 mm) from Aluminum on Steel Rotary Mechanism After Exposure to 40 mg/litre of Contaminant (Magnification = 100X).

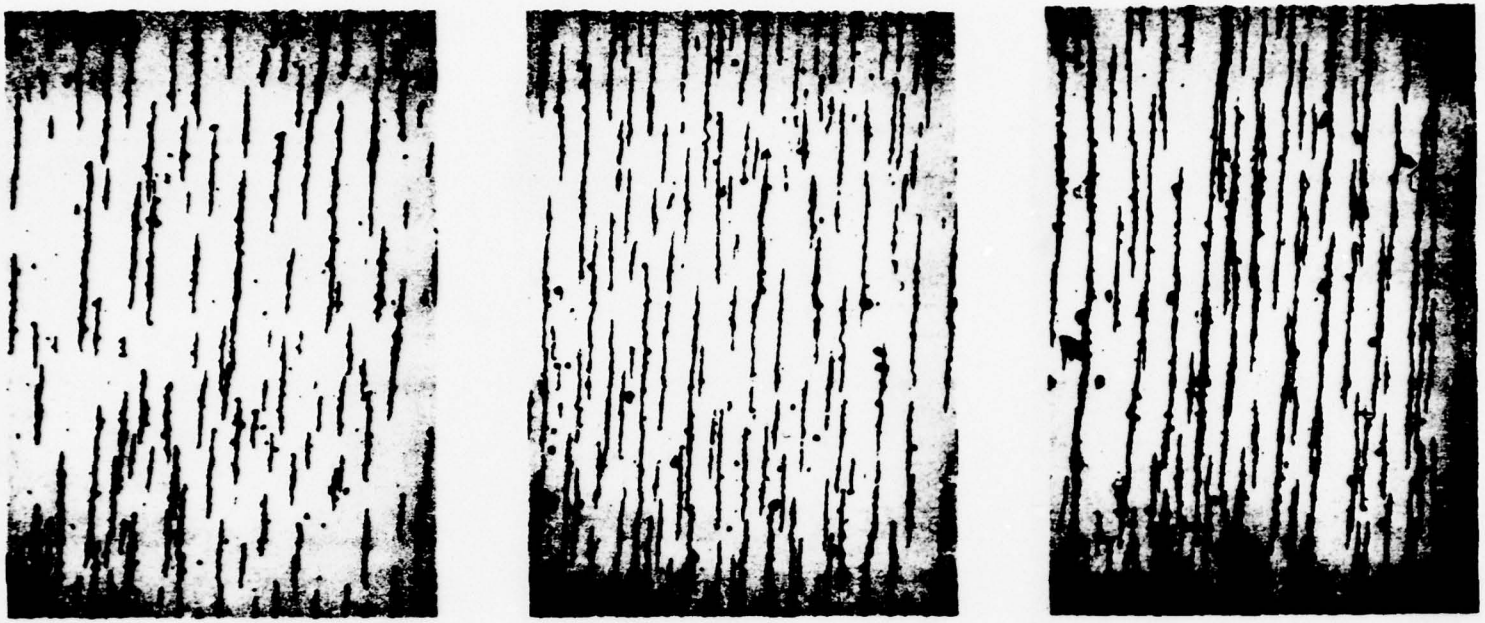

(a)

After Exposure to 0-5 μM Particle Size Range (Volume = 3 ml)

(b)

After Exposure to 0-30 μM Particle Size Range (Volume = 3 ml)

(c)

After Exposure to 0-80 μM Particle Size Range (Volume = 3 ml)

Fig. 29. Ferrograms of Wear Debris (54 mm) from Aluminum on Steel Rotary Mechanism After Exposure to 80 mg/litre of Contaminant (Magnification = 100X).

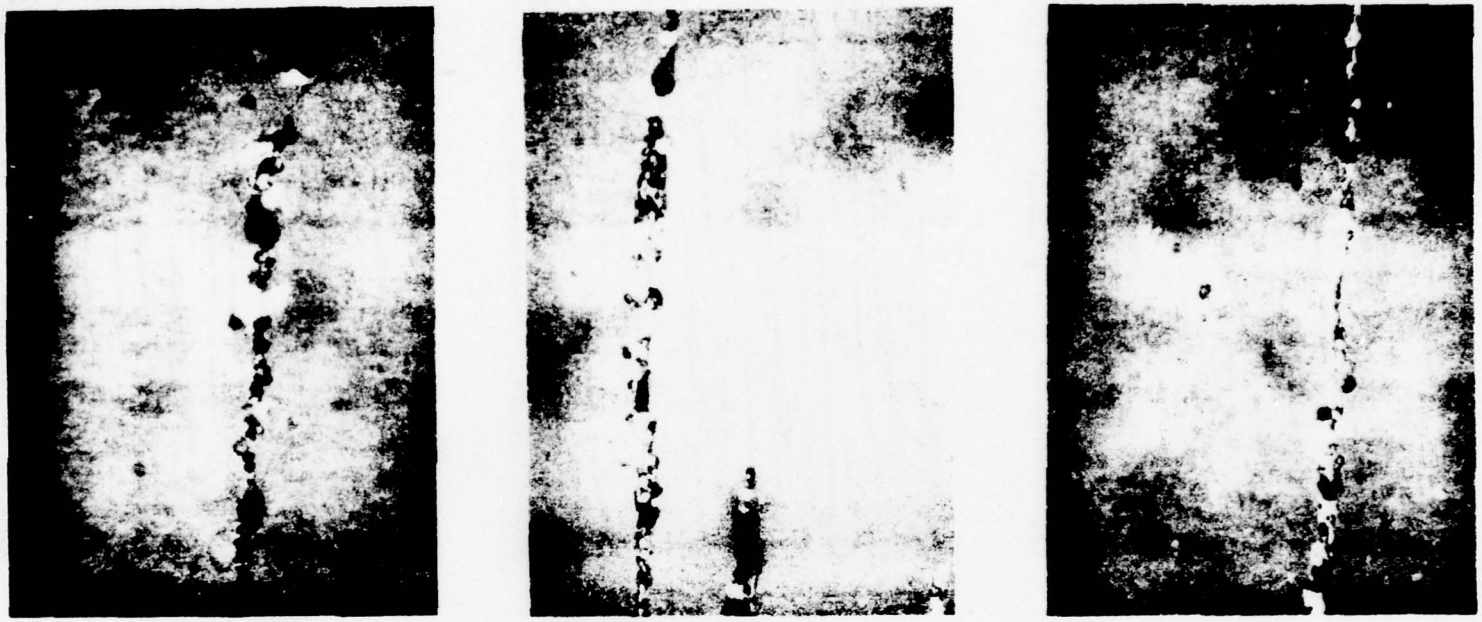

(a)

After Exposure to 0-5 μM Particle Size Range (Volume = 12 ml)

(b)

After Exposure to 0-30 μM Particle Size Range (Volume = 12 ml)

(c)

After Exposure to 0-80 μM Particle Size Range (Volume = 12 ml)

Fig. 30. Ferrograms of Wear Debris (54 mm) from Aluminum on Steel Rotary Mechanism After Exposure to 5 mg/litre of Contaminant (Magnification = 1000X).

(a)

After Exposure to 0-5 μM Particle Size Range (Volume = 12 ml)

(b)

After Exposure to 0-30 μM Particle Size Range (Volume = 12 ml)

(c)

After Exposure to 0-80 μM Particle Size Range (Volume = 12 ml)

Fig. 31. Ferrograms of Wear Debris (54 mm) from Aluminum on Steel Rotary Mechanism after Exposure to 10 mg/litre of Contaminant (Magnification = 1000X).

(a)

After Exposure to 0-5 μM Particle Size Range (Volume = 12 ml)

(b)

After Exposure to 0-30 μM Particle Size Range (Volume @ 12 ml)

(c)

After Exposure to 0-80 μM Particle Size Range (Volume = 12 ml)

Fig. 32. Ferrograms of Wear Debris (54 mm) from Aluminum on Steel Rotary Mechanism After Exposure to 20 mg/litre of Contaminant (Magnification = 1000X).

(a)

After Exposure to 0-5 μM Particle Size Range (Volume = 6 ml)

(b)

After Exposure to 0-30 μM Particle Size Range (Volume = 6 ml)

(c)

After Exposure to 0-80 μM Particle Size Range (Volume = 6 ml)

Fig. 33. Ferrograms of Wear Debris (54 mm) from Aluminum on Steel Rotary Mechanism After Exposure to 40 mg/litre of Contaminant (Magnification = 1000X).

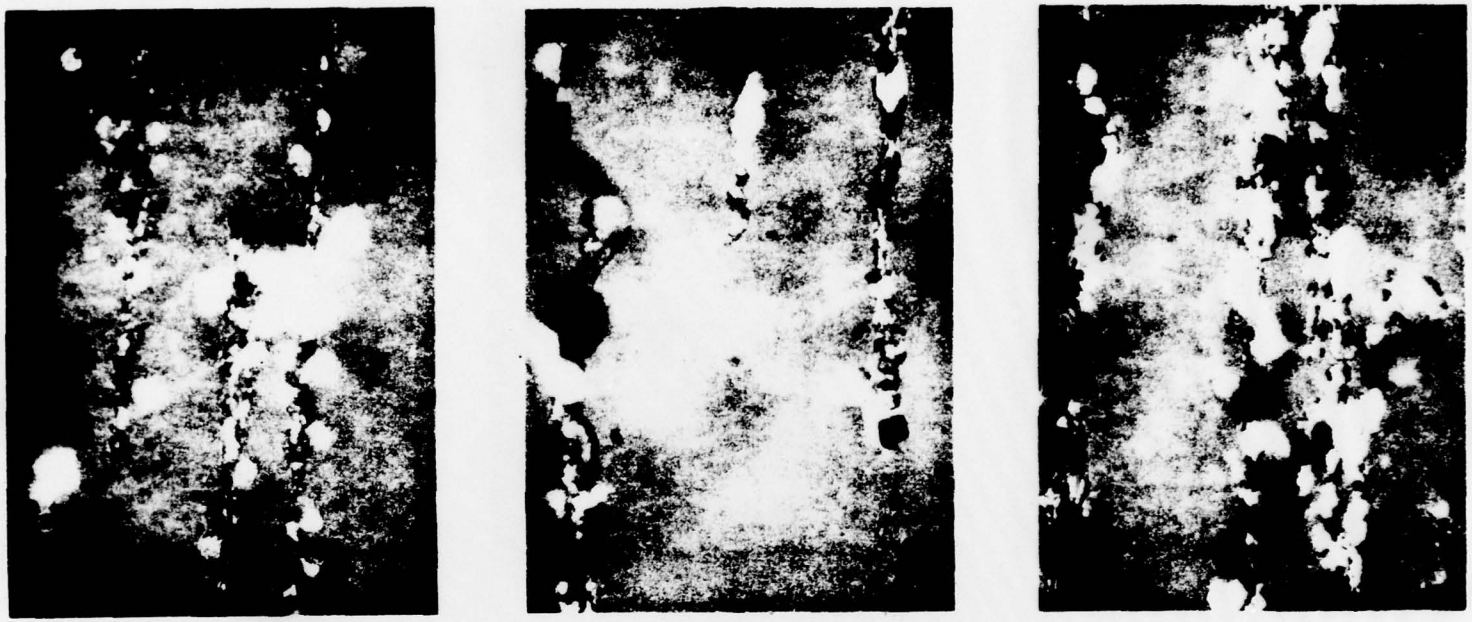

(a)

After Exposure to 0-5 μM Particle Size Range (Volume = 3 ml)

(b)

After Exposure to 0-30 μM Particle Size Range (Volume = 3 ml)

(c)

After Exposure to 0-80 μM Particle Size Range (Volume = 3 ml)

Fig. 34. Ferrograms of Wear Debris (54 mm) from Aluminum on Steel Rotary Mechanism After Exposure to 80 mg/litre of Contaminant (Magnification = 1000X).

VI. LINEAR MECHANISM

Description

The linear mechanism was designed to simulate relative motion as found in a piston/bore combination of a piston pump or a spool valve. In general dimensions, it is modeled after a spool valve having a bore and stroke dimensionally typical of such a mechanism. Figure 35 depicts the linear mechanism without the drive mechanism. As shown, contaminated fluid enters the central chamber at test pressure. Note that flow forces on the spool are balanced by a second entry port 180° from the first. Two outlet ports are placed 90° from the inlets. Upon entering the mechanism, the fluid divides into a flow stream through the outlets and a leakage flow between the spool and bore. Leakage flow is plumbed back to the main return line at a point downstream of the pressure drop valve located on the main return line just past the mechanism outlet. The leakage lines are valves in order that their combined flow may be diverted to a sample tube. The test specimens themselves consist of three sets of one spool of 1020 mild steel and two matched bores of cast iron. Bore diameters are nominally 12.70 millimetres, and spool ends are lapped to individual bore diameters minus 10 micrometres. Each matched set of three pieces was utilized for one particle size range of test dust at various, increasing concentrations.

LINEAR MECHANISM

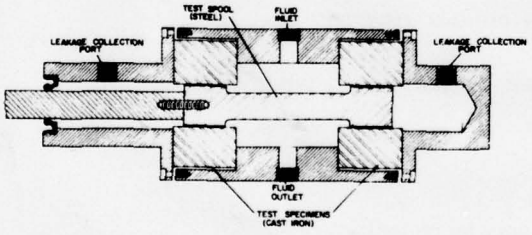

Fig. 35. Schematic of Linear Mechanism.

Leakage flow between spool and bores was monitored when sampling as a trend indicator. Theoretically, the flow may be expressed (from Ref. [22]) as:

$$Q = k_5 \pi \frac{R b^3 \Delta P}{\mu L} [1 + 1.5 (\epsilon/b)^2] \qquad (18)$$

where:
- Q = volumetric flow
- R = spool radius
- b = radial clearance
- ΔP = pressure differential
- μ = dynamic viscosity
- L = passage length
- ϵ = eccentricity between spool and bore
- k_5 = constant for annular passage

During the actual test, the linear mechanism is in motion. Equation (18), however, holds only for the static case; so, a motion-induced flow must also be considered. The velocity profile of a motion-induced flow between two flat plates may be expressed (from Ref. [22]) as:

$$u = v\,(1/2 + (2z/b)) \tag{19}$$

where: u = fluid velocity
z = distance from center of gap in radial direction
v = relative velocity of plates

In the case of the rotary mechanism with eccentricity of spool and bore center, the gap height becomes:

$$h_L = (b-\epsilon) + \frac{2\epsilon\phi}{\pi} \tag{20}$$

where: h_L = gap height at any angle ϕ
ϕ = angle from minimum gap $(0 < \phi < \pi)$

Total motion-induced flow may be found by integrating velocity over gap height and width:

$$Q_v = udA$$
$$Q_v = k_6\,\pi\,Rbv \tag{21}$$

where: k_6 = constant for annular passage.

The velocity, V, imparted by the scotch yoke mechanism is:

$$V = r_o\,\omega\,\theta \tag{22}$$

where: r_o = yoke radius
ω = drive shaft angular velocity
θ = angle from vertical of yoke

The flows in such a small clearance may be assumed laminar; therefore, using super-

$$Q_t = k_7\,\pi\,Db^3 \left\{ \frac{\Delta P}{\mu L} \left[1 + 1.5\,(\epsilon/b)^2 \right] + \frac{6r\omega\,\sin\theta}{b^2} \right\} \tag{23}$$

where: Q_t = total volumetric flow
k_7 = constant for annular passage

The final equation depicts a pulsating flow due to the oscillation of the piston. The flow equations for both the linear and rotary mechanisms illustrate the complexity of the contaminant wear/component performance inter-relationship. Note that, in both cases, the flow is a cubic function of the clearance. This implies that there should be large changes in leakage flow for small changes in dimensions (i.e., low wear). The potential for disastrous contaminant wear situations is evident.

Test Procedure

As in the case of the rotary mechanism, the linear mechanism underwent a break-in period. The procedure not only served to break-in the mechanism but also to check the drive mechanism for alignment and proper operation. The break-in procedure was as follows:

1. **Install oil-wetted specimen set (spool and bores) in mechanism.**
2. **Connect drive mechanism and check for proper alignment.**
3. **Operate stand until proper oil temperature is achieved, set proper flow through mechanism (mechanism not reciprocating), and set pressure to 25% of test pressure.**
4. **Activate mechanism and operate for 15 minutes.**
5. **Increase pressure by 25% of test pressure and operate for 15 minutes.**
6. **Repeat 5 until test pressure is achieved.**
7. **Operate at full test pressure for one hour.**

At the end of this one hour and 45 minute period, the linear mechanism's test parameters were established. The parameters held constant are listed in Table III. Note that a comparison of Tables I and III illustrates an important difference between the rotary and linear mechanism tests; that is, the constant test clearance of the rotary mechanism versus the varying clearance of the linear mechanism tests. As described by the equations depicting the theoretical flow through the annular clearance of the linear mechanism over a long time interval, the pulsating effect (from the reciprocating motion) integrates to zero, leaving the leakage flow a function only of the cube of the clearance. Therefore, the leakage flow rate provided a secondary indication of the wear (i.e., clearance change) in the mechanism. The test procedure was as follows:

1. **Install specimens and conduct break-in.**
2. **Establish test flow, pressure, and temperature with filters in system and activate mechanism.**
3. **Remove filters from flow loop.**
4. **Inject 5 milligrams/litre of 0-5 micrometre ACFTD.**
5. **Circulate oil with contaminant for 14 minutes, taking samples at 2, 4, 8, and 14 minutes.**
6. **Filter circulating oil for 30 minutes.**
7. **Repeat Steps 3-6 for concentrations of 10, 20, 40, and 80 milligrams per litre.**
8. **Repeat Steps 1 through 7 for 0-30 and 0-80 micrometre contaminants.**

TABLE III. Summary of Test Parameters Held Constant During Linear Mechanism Tests.

Symbol	Description	Value
ΔP	Pressure Drop Across Test Clearance	1000 psi
ω	Cycle Rate of Mechanism	85 Cycles Per Minute
T	Fluid Temperature	120°F
Q	Total Fluid Flow Rate Through Mechanism	3.0 gpm

This procedure produced a set of tests as delineated in Table IV.

TABLE IV. Summary of Linear Mechanism Tests.

Specimen Number	Material	Contaminant Size (micrometres)	Contaminant Concentration (milligrams/litre)
1-C	Cast Iron	0-5	5, 10, 20, 40, 80
2-C	Cast Iron	0-5	5, 10, 20, 40, 80
3-C	Cast Iron	0-80	5, 10, 20, 40, 80

Following the rotary mechanism example, each individual specimen set was subjected to increasing concentrations of one contaminant size range. Since the diameters of the test specimen bore and spool differed by 10 micrometres, the nominal clearance was 5 micrometres. Therefore, the 0-5, 0-30, and 0-80 micrometre contamination represented contaminant that was the same size, larger than, and much larger than the clearance, respectively.

Test Results

The amount of metallic debris, as measured by Ferrographic densities, was used as the prime indicator of wear in the linear mechanism. In the same manner as reported

for the rotary mechanism, Fig. 36 plots the normalized Ferrographic densities, D54 per millilitre, against contaminant concentration in milligrams per litre. The linear mechanism test results also follow the rotary's in that the least amount of wear is produced by the 0-5 micrometre cut, more by the 0-30 micrometre contaminant, and the greatest by the largest dust size, 0-80 micrometres. Again, the curves converge rather rapidly in the low contamination concentrations, implying that particle size distribution is less of a factor in low contaminant concentrations.

The effect of the contaminant on each of the specimens may be seen in Fig. 37, which is a set of photographs of each spool used. Note the similarity to Figs. 13 and 14, in that the least amount of damage was done by the 0-5 micrometre contaminant, much more severe scoring is evident in the photo of the 0-30 micrometre sample, and exposure to 0-80 micrometre dust results in an extremely rough surface. This last fact is dramatized by the darkness of the 0-80 photograph, even though the exposure time was identical to the 0-5 and 0-30 pictures. Figures 38-42 as a set depict the 54 millimetre location on each 14-minute sample (used in all data). Again, the reader should be cautioned not to attempt conclusions based on the relative amounts of debris appearing due to disparities in sample volumes. A closer look at the debris in the high magnification microphotographs of Figs. 43-47 reveals much more detail. Immediately evident are the larger wear particles of the 0-30 micrometre tests and the greater incidence of cutting wear in the 0-30 and 0-80 micrometre samples. These cutting wear particles are indicative of *"large"* contaminant particles and *"small"* wearing clearances. Other differences in the amount of wear debris produced by the linear versus rotary mechanism become apparent only when the results of last year's tests at a larger clearance are integrated into these data.

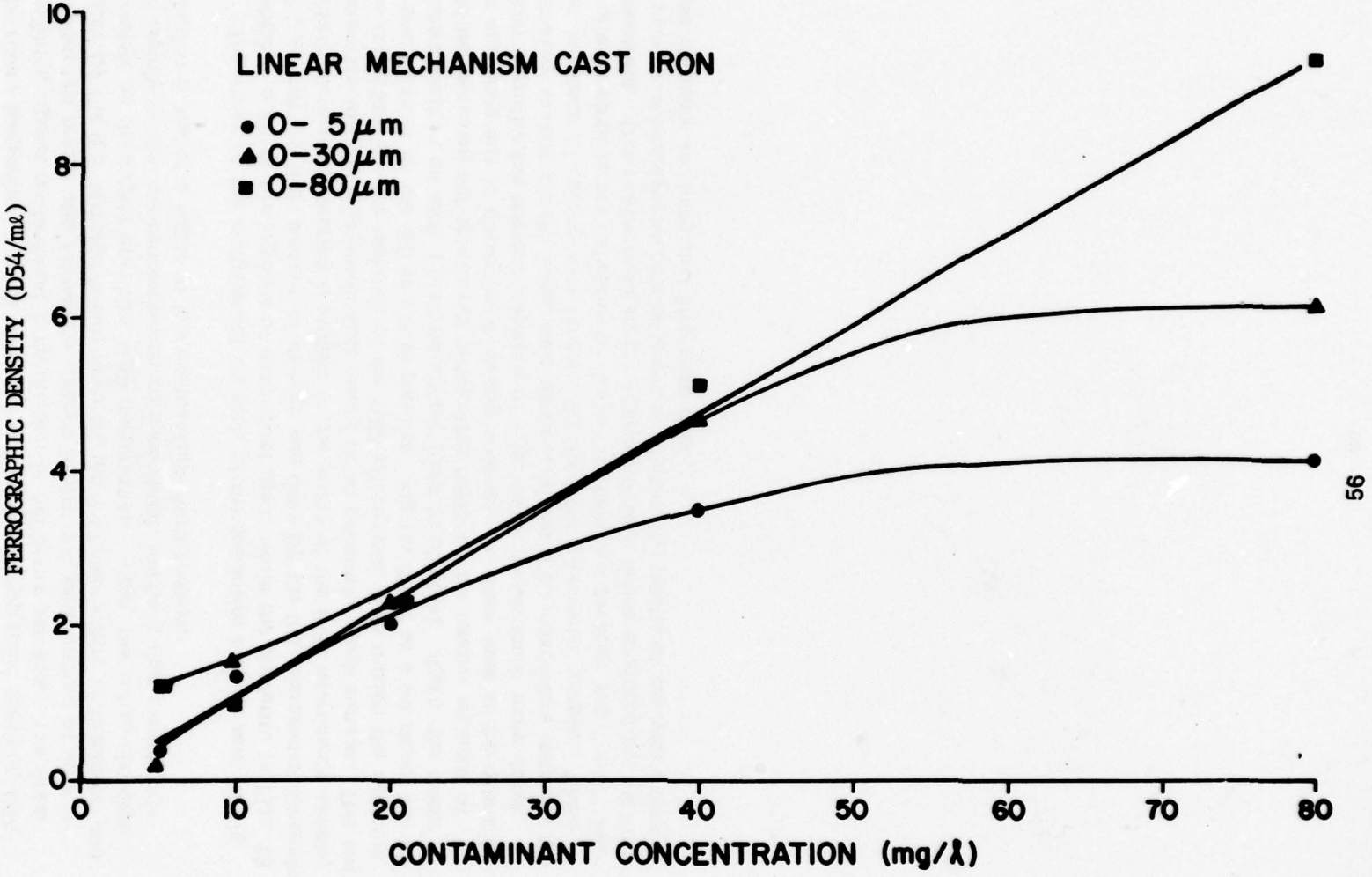

Fig. 36. Test Results – Linear Mechanism – Cast Iron/Steel Specimen.

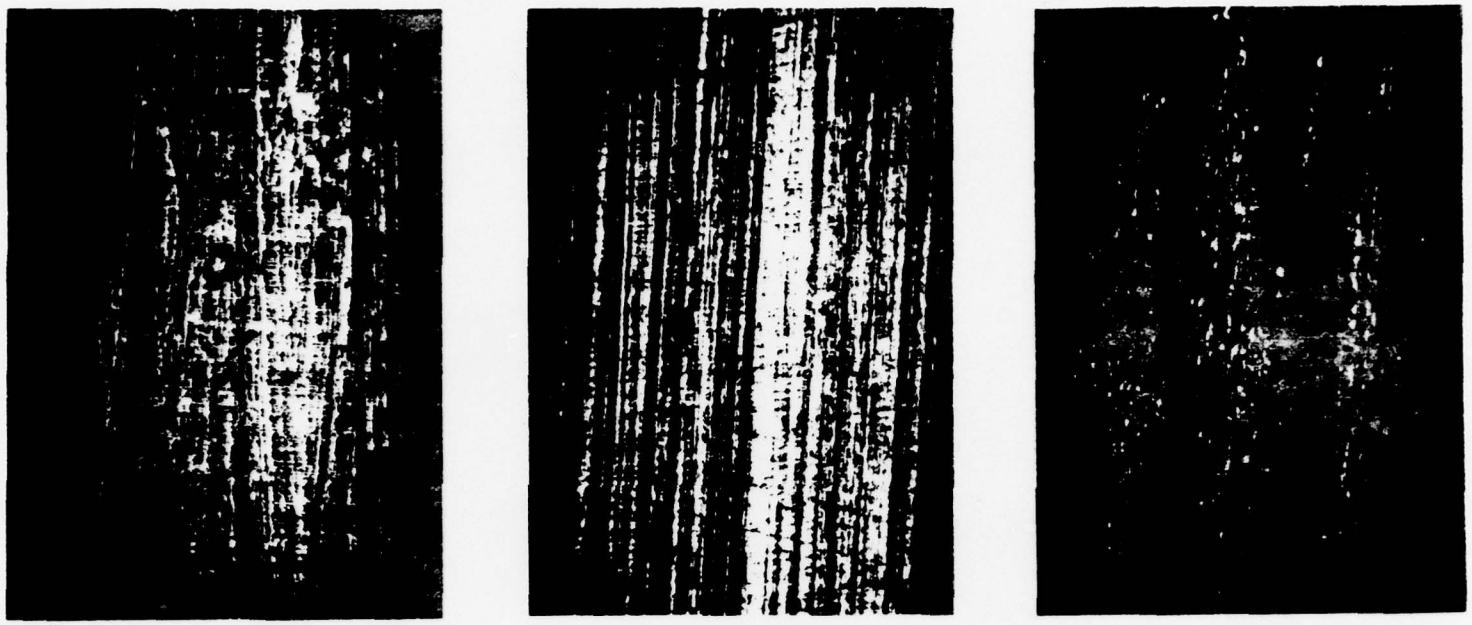

(a)

After Exposure to 0-5 μM
Particle Size Range

(b)

After Exposure to 0-30 μM
Particle Size Range

(c)

After Exposure to 0-80 μM
Particle Size Range

Fig. 37. Surface of Steel Linear Mechanism Spool After Contaminant Exposure (Magnification = 50X).

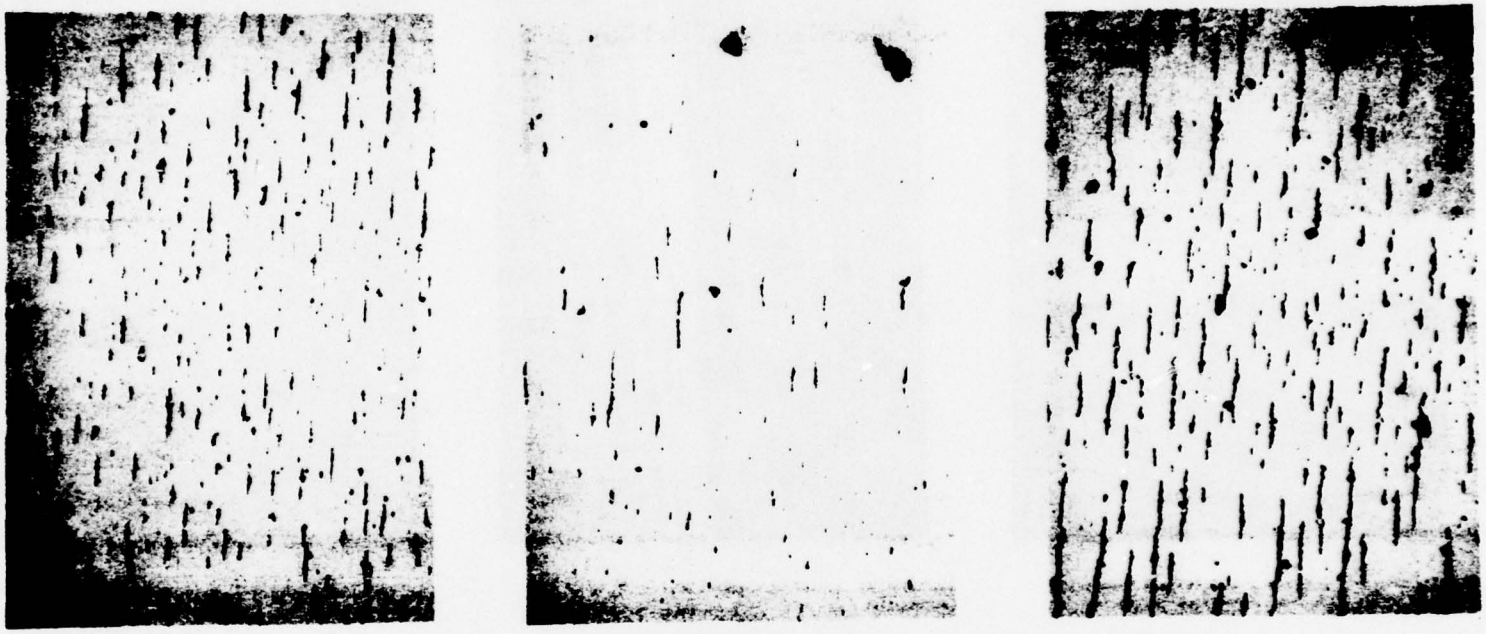

(a)

After Exposure to 0-5 μM Particle Size Range (Volume = 12 ml)

(b)

After Exposure to 0-30 μM Particle Size Range (Volume = 12 ml)

(c)

After Exposure to 0-80 μM Particle Size Range (Volume = 6 ml)

Fig. 38. Ferrograms of Wear Debris (54 mm) from Linear Mechanism After Exposure to 5 mg/litre of Contaminant (Magnification = 100X).

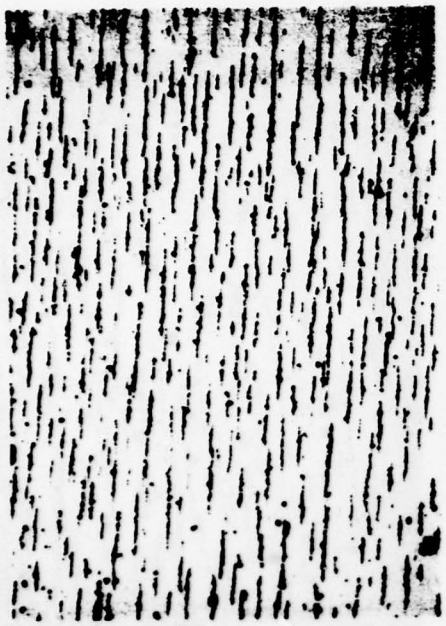

(a)

After Exposure to 0-5 μM Particle Size Range (Volume = 12 ml)

(b)

After Exposure to 0-30 μM Particle Size Range (Volume = 12 ml)

(c)

After Exposure to 0-80 μM Particle Size Range (Volume = 12 ml)

Fig. 39. Ferrograms of Wear Debris (54 mm) from Linear Mechanism After Exposure to 10 mg/litre of Contaminant (Magnification = 100X).

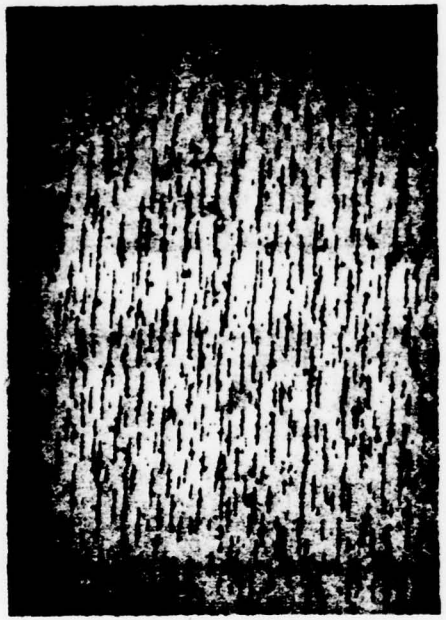

(a)

After Exposure to 0-5 μM Particle Size Range (Volume = 12 ml)

(b)

After Exposure to 0-30 μM Particle Size Range (Volume = 6 ml)

(c)

After Exposure to 0-80 μM Particle Size Range (Volume = 12 ml)

Fig. 40. Ferrograms of Wear Debris (54 mm) from Linear Mechanism After Exposure to 50 mg/litre of Contaminant (Magnification = 100X).

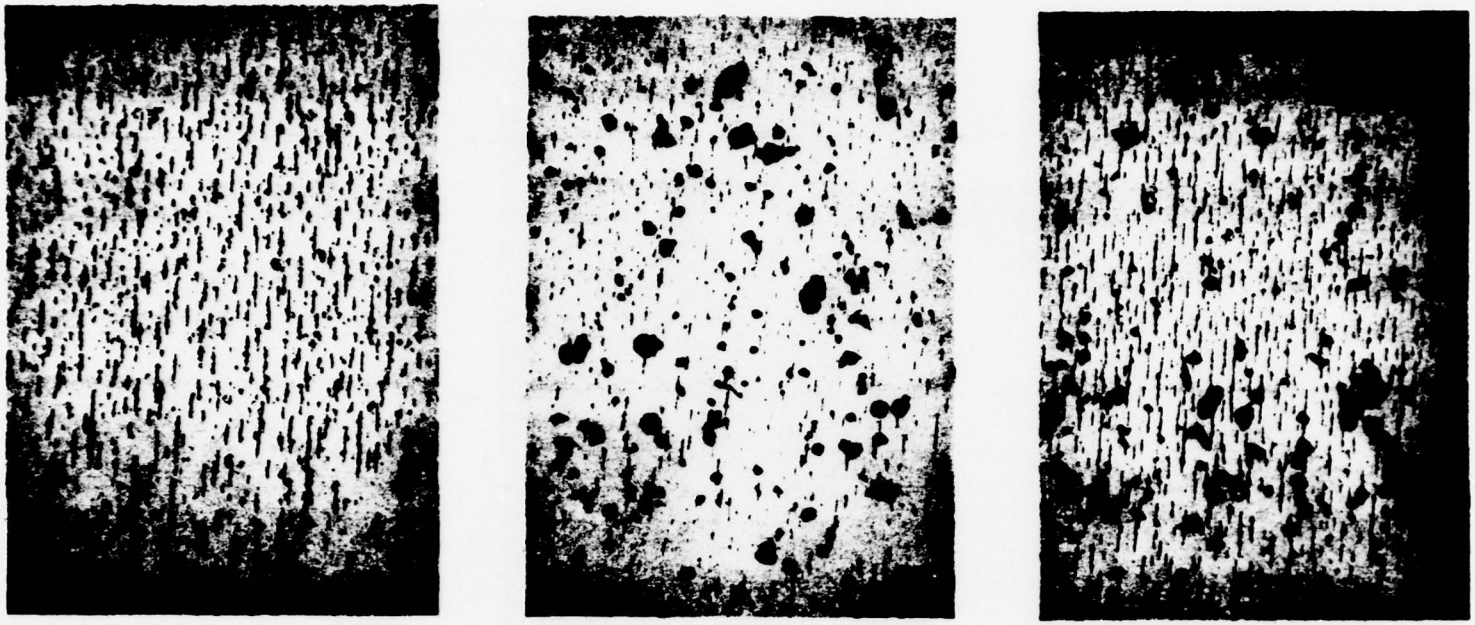

(a)

After Exposure to 0-5 μM Particle Size Range (Volume = 6 ml)

(b)

After Exposure to 0-30 μM Particle Size Range (Volume = 6 ml)

(c)

After Exposure to 0-80 μM Particle Size Range (Volume = 6 ml)

Fig. 41. Ferrograms of Wear Debris (54 mm) from Linear Mechanism After Exposure to 40 mg/litre of Contaminant (Magnification = 100X).

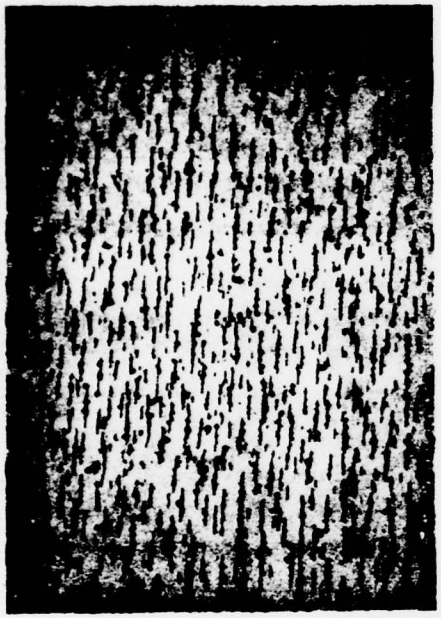

(a)

After Exposure to 0-5 μM Particle Size Range (Volume = 6 ml)

(b)

After Exposure to 0-30 μM Particle Size Range (Volume = 6 ml)

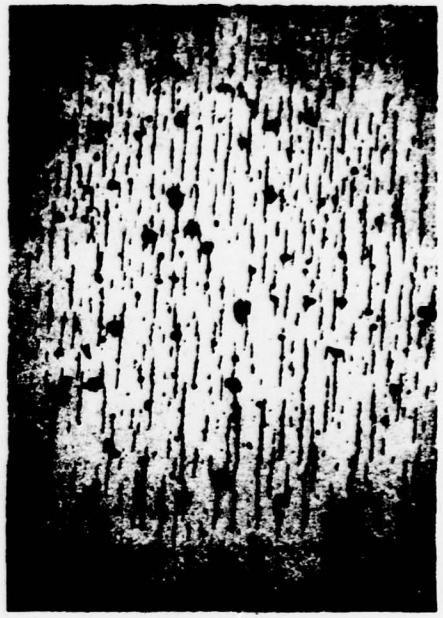

(c)

After Exposure to 0-80 μM Particle Size Range (Volume = 3 ml)

Fig. 42. Ferrograms of Wear Debris (54 mm) from Linear Mechanism After Exposure to 80 mg/litre of Contaminant (Magnification = 100X).

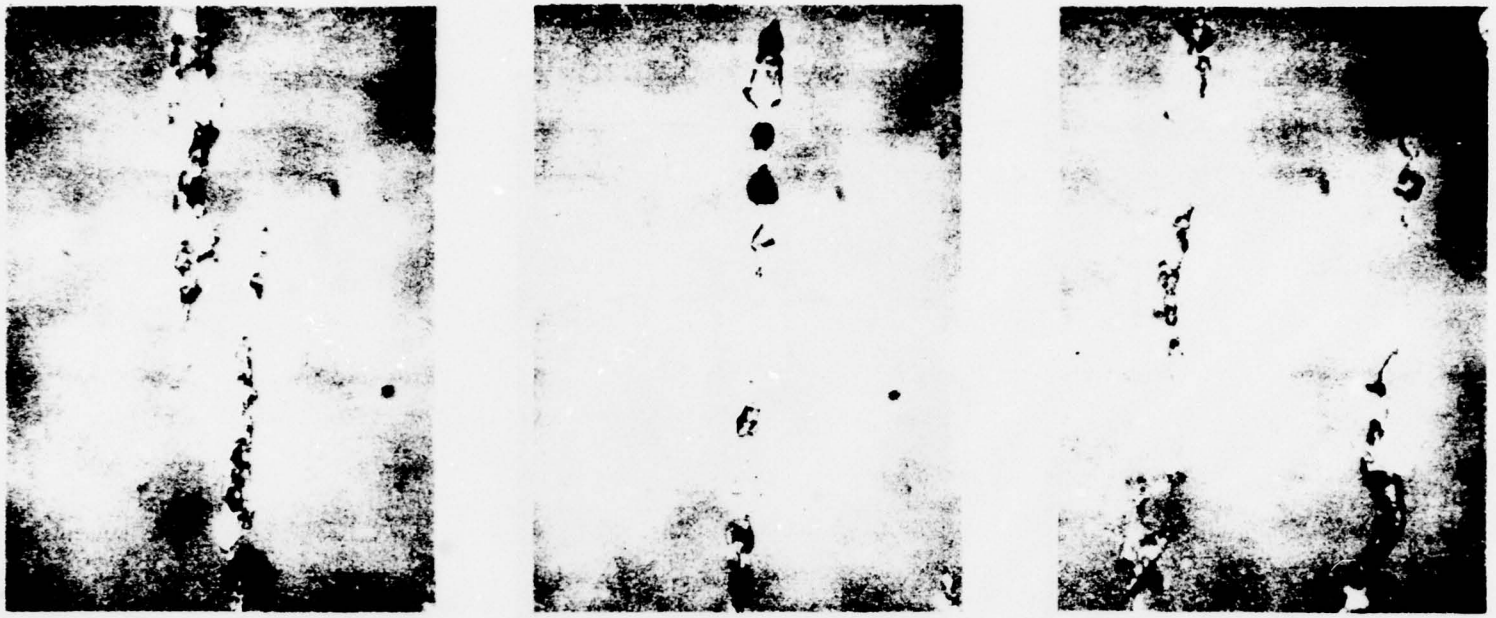

(a)

After Exposure to 0-5 μM Particle Size Range (Volume = 12 ml)

(b)

After Exposure to 0-30 μM Particle Size Range (Volume = 12 ml)

(c)

After Exposure to 0-80 μM Particle Size Range (Volume = 6 ml)

Fig. 43. Ferrograms of Wear Debris (54 mm) from Linear Mechanism After Exposure to 5 mg/litre of Contaminant (Magnification = 1000X).

(a)

After Exposure to 0-5 μM Particle Size Range (Volume = 12 ml)

(b)

After Exposure to 0-30 μM Particle Size Range (Volume = 12 ml)

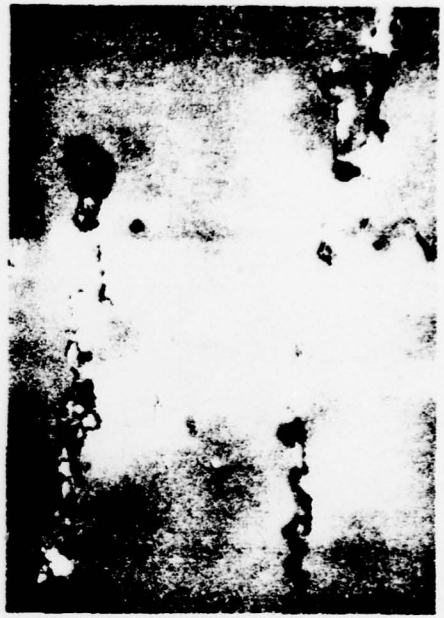

(c)

After Exposure to 0-80 μM Particle Size Range (Volume = 12 ml)

Fig. 44. Ferrograms of Wear Debris (54 mm) from Linear Mechanism After Exposure to 10 mg/litre of Contaminant (Magnification = 1000X).

(a)

After Exposure to 0-5 μM Particle Size Range (Volume = 12 ml)

(b)

After Exposure to 0-30 μM Particle Size Range (Volume = 6 ml)

(c)

After Exposure to 0-80 μM Particle Size Range (Volume = 12 ml)

Fig. 45. Ferrograms of Wear Debris (54 mm) from Linear Mechanism After Exposure to 20 mg/litre of Contaminant (Magnification = 1000X).

(a)

After Exposure to 0-5 μM Particle Size Range (Volume = 6 ml)

(b)

After Exposure to 0-30 μM Particle Size Range (Volume = 6 ml)

(c)

After Exposure to 0-80 μM Particle Size Range (Volume = 6 ml)

Fig. 46. Ferrograms of Wear Debris (54 mm) from Linear Mechanism After Exposure to 40 mg/litre of Contaminant (Magnification = 1000X).

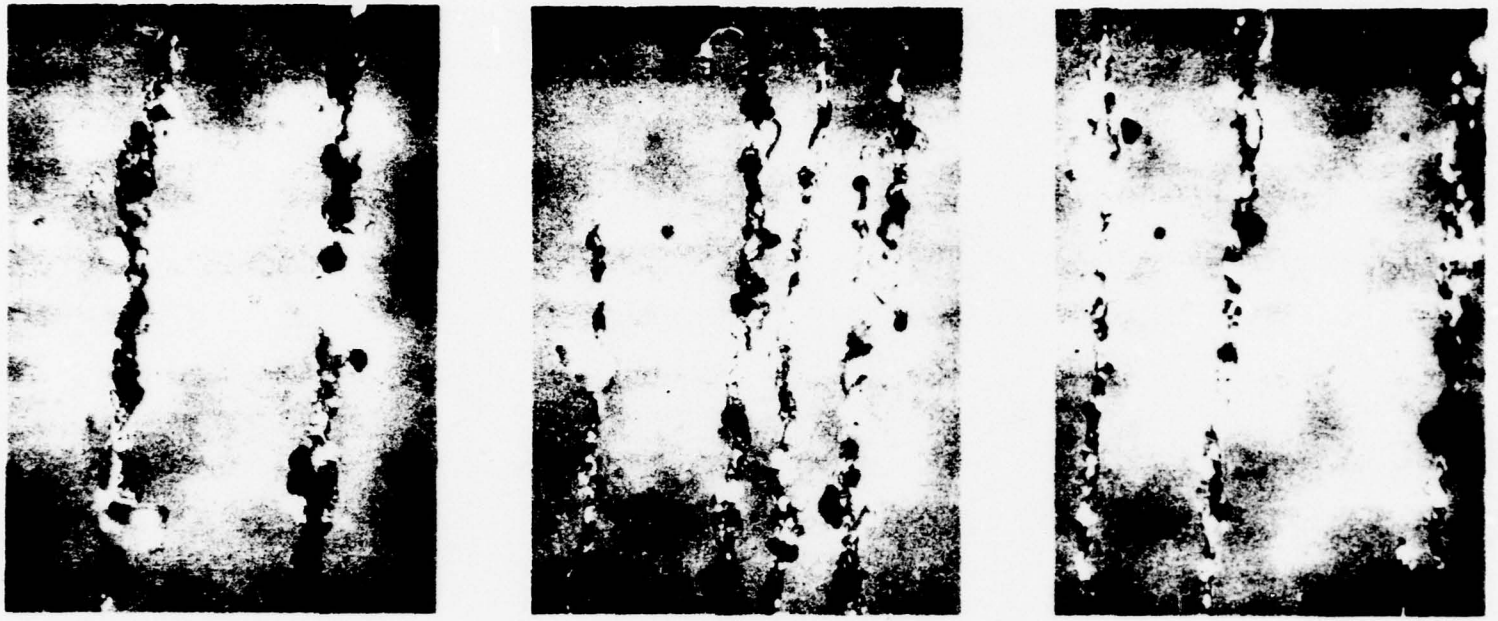

(a)

After Exposure to 0-5 μM Particle Size Range (Volume = 6 ml)

(b)

After Exposure to 0-30 μM Particle Size Range (Volume = 6 ml)

(c)

After Exposure to 0-80 μM Particle Size Range (Volume = 3 ml)

Fig. 47. Ferrograms of Wear Debris (54 mm) from Linear Mechanism After Exposure to 80 mg/litre of Contaminant (Magnification = 1000X).

VII. DISCUSSION OF OVERALL MECHANISM RESULTS

The rotary mechanism tests were conducted with a clearance held constant throughout the test duration. This reflects a situation often realized in actual components of a wear-compensating design. The data, however, do not represent what is occurring when the wearing clearance undergoes a dimensional change due to that wear.

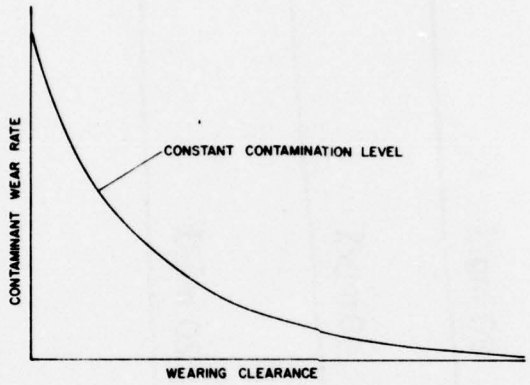

Fig. 48. Theoretical Contaminant Wear Rate versus Wearing Clearance for Constant Contamination Level.

Figure 48 depicts the theoretical wear rate with respect to clearance for a constant contamination level. Note that, as the clearance decreases from some large value, the rate of contaminant wear increases. A simplified explanation of this situation might be that each contaminant particle takes a larger and larger *"bite"* out of the wearing surface until, at zero clearance, each particle is achieving its maximum damage potential. At the other end of the scale, the clearance would be so great that all contaminant particles would pass unimpeded. In this case, abrasive wear would drop to a zero level, leaving only the erosive wear mode. Note that this curve is based on the assumption that all contaminant particles are forced through the test clearance, regardless of their size. In the Fluid Power Research Center's rotary mechanism, this was indeed the case, since the flow divider was designed to split the oil flow into two streams representative of the system contamination level. Therefore, the curve of Fig. 48 should be a good indicator of the test data curves. The test results do bear out this concept, as shown by Figs. 49 and 50, depicting the wear rate versus test clearance at constant contamination concentrations for the brass/steel and aluminum/steel specimens, respectively. The reader will note that both figures present the same message of increasing wear rate with decreasing clearance. The non-dimensional factor of h/D, where h is the test clearance and D is the largest dimension in a contaminant size range, allows the data from the 0-5, 0-30, and 0-80 micrometre contaminant tests to be plotted on the same figure in the form of a constant contamination concentration trace. There is some

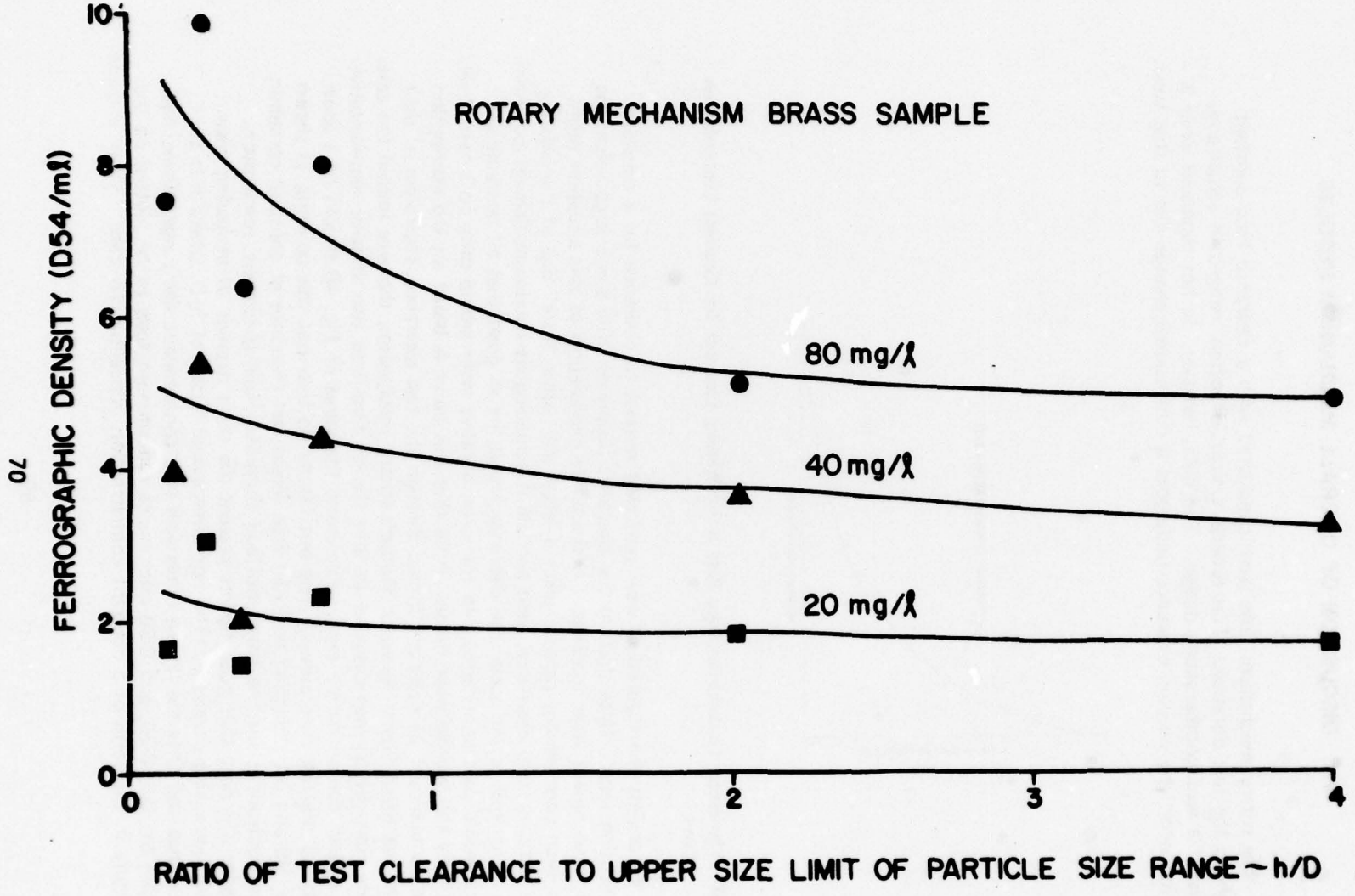

Fig. 49. Wear Rate vs. Varying Test Clearance at Constant Contaminant Concentrations (Brass/Steel Rotary Mechanism Tests).

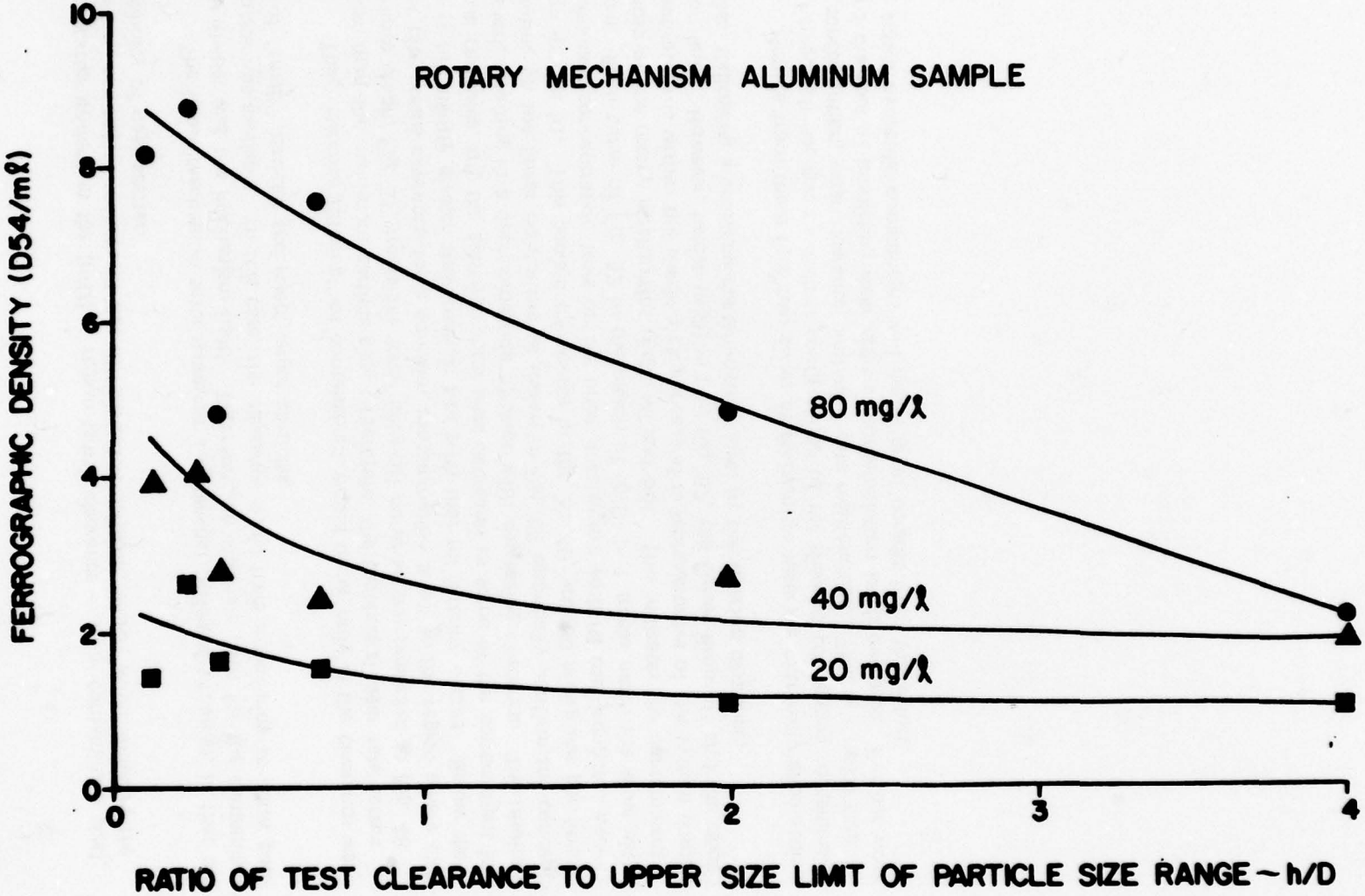

Fig. 50. Wear Rate vs. Varying Test Clearance at Constant Contamination Concentrations (Aluminum/Steel Rotary Mechanism Tests).

data scatter evident in the (h/D) < region (small clearance – large contaminant size); however, control of such small size differences is difficult, which would enhance the possibility of data scatter.

The linear mechanism tests represent a somewhat different situation, in that the flow divider was the mechanism itself. Therefore, an alternate path for the contaminant particles was available. In this case, the clearance could have a tendency to allow passage of *"small"* particles and reject larger particles.

This *"selective filtering"* of contaminant would occur only if the clearance was smaller than the maximum particle size. Therefore, the theoretical wear rate versus clearance graph, Fig. 51, traces the same (shaped) curve as was presented in Fig. 48 (wear rate versus clearance for a constant contamination level) in the region where clearance is sufficiently greater than particle size such that no filtering occurs. Below the critical clearance, h*, the contamination level decreases as some of the contaminant is removed, resulting in a decreasing rate of wear with decreasing clearance. The results of testing on the linear mechanism as shown in Fig. 52 essentially confirm the concept shown in Fig. 51. This depicts the results of the 20, 40, and 80 milligrams per litre contaminant concentration tests on the linear mechanism with its cast iron/steel wear sample. Each curve of Fig. 52 in the region of (h/D) > 1 traces much the same path as those of the rotary mechanisms (Figs. 49 and 50). This indicates the contaminant concentration is within the wearing clearance and is representative of the system contamination level. However, below (h/D) = 1 in Fig. 52, the curves drop off and the slope reverses, indicating a changing contamination level in the wearing clearance.

Results from these first two series of mechanism tests are extremely encouraging. The Ferrograph has given excellent confirmation of the theories concerning contaminant size, concentration, wear clearance, and wear rate relationships. This is a major step toward the goal of predicting wear rates as contamination levels decrease. Further work using actual hydraulic components will derive great benefit from this effort.

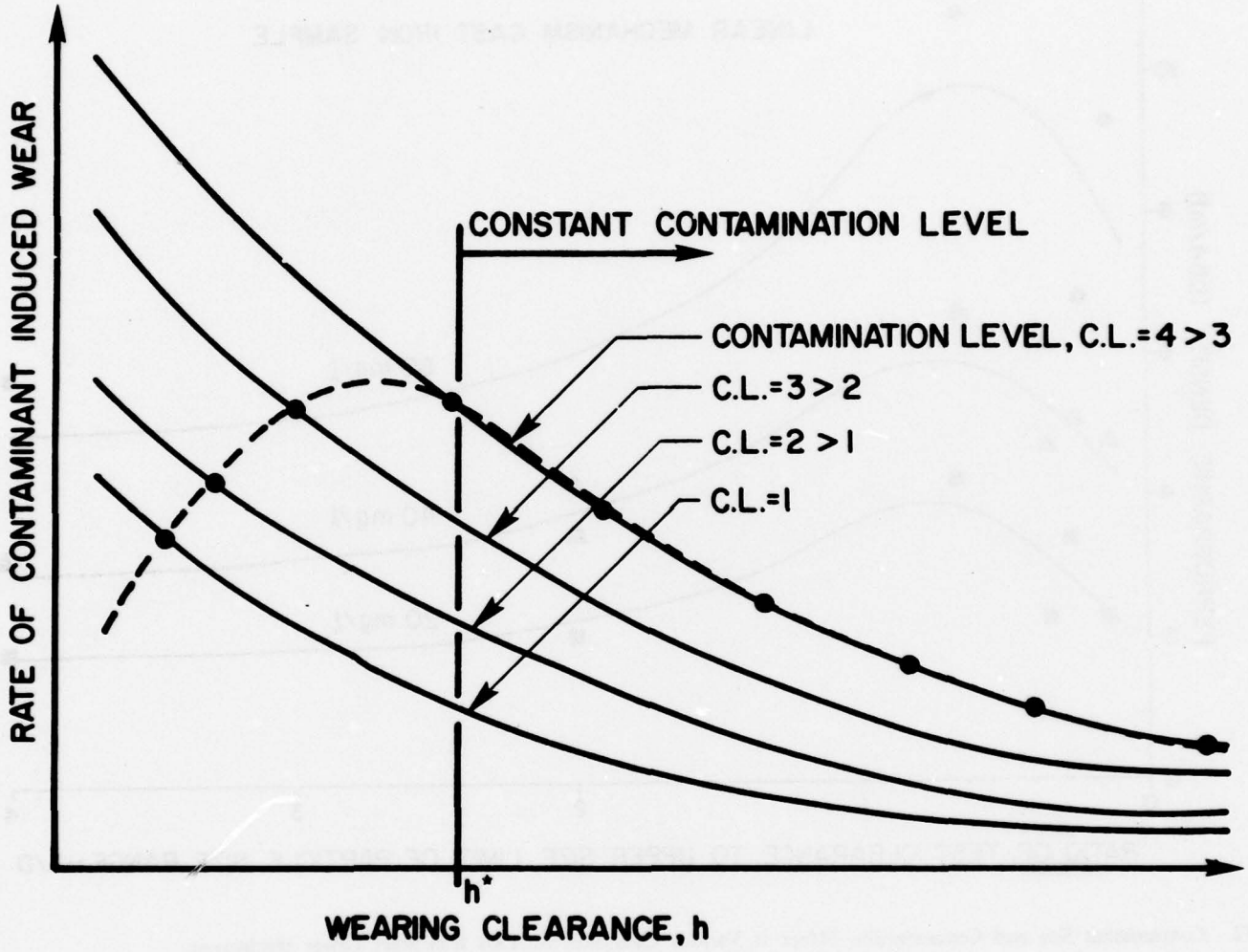

Fig. 51. Rate of Contaminant-Induced Wear vs. Wearing Clearance for Linear Mechanism, Including Effect of Varying Contamination Level.

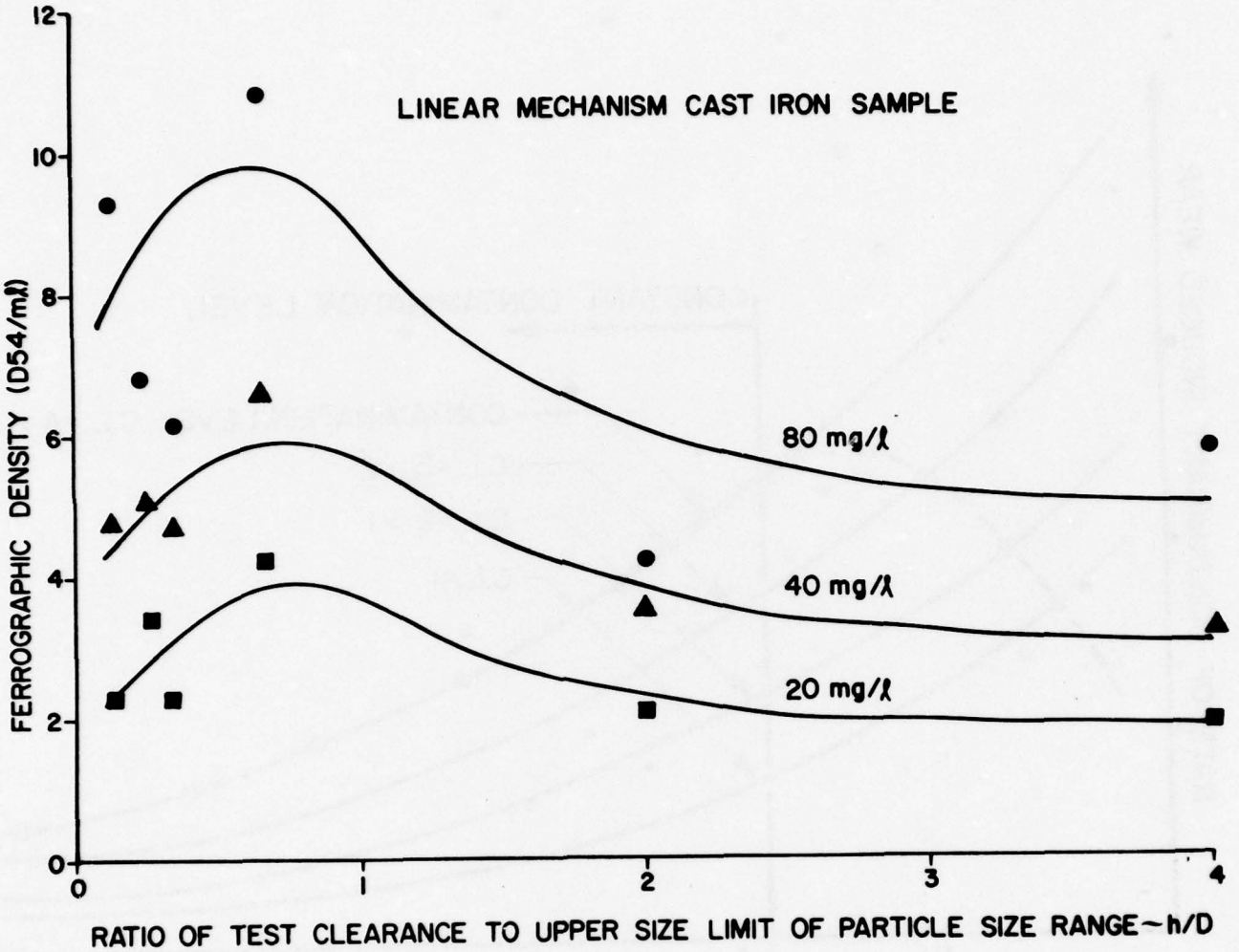

Fig. 52. Contaminant Size and Concentration Effect at Various Clearances on Cast Iron/Steel Linear Mechanism.

VIII. COMPONENT TESTS

Description

One of the most widely used pump designs in today's fluid power systems is that of the hydraulic gear pump. Therefore, the positive displacement gear pump was selected for analysis in this program. The effects of contaminant wear within these gear pumps are primarily centered around the change of flow through internal critical leakage paths which exist. As particulate contaminant flows through these passages, surface material is removed, allowing leakage flow to increase and, correspondingly, pump output flow to degrade. Since it is practically impossible to measure the dimensional changes to these internal clearances, a relationship between the amount of wear debris (measured Ferrographically) generated and flow degradation is therefore necessary.

Previous studies have shown that there are three major leakage paths inherent to hydraulic gear pumps [23, 24, 25, 26]. Thus investigation into the contaminant wear within these passages should provide an insight to increased pump flow degradation. Figure 53 shows the schematic cross-section of a gear pump, with Q_1, Q_2, and Q_3 defining the leakage flow through these three paths. The first leakage path can be described by the passage between the side of the gears and the surface of the wear plate. In this path, however, it is highly unlikely that significant dimensional changes will occur to the length and width (changes in root diameter and shaft diameter). Thus, any wear which occurs will result in changes in the clearance between the wear plate and the side of the gears. The wear debris generated here can now be considered a direct function of the clearance change in this path.

A similar result is obtained for the second leakage path, in which leakage flow Q_2 is observed. Here, the width and length of this path are dependent upon the distance between the gear shafts and the gear teeth meshing area, respectively, and should not appreciably change with the presence of particulate contaminant. Therefore, wear material removed within this passage can also be directly related to the resulting clearance change of this path.

The third leakage path can be described by the clearance between the gear teeth and the internal wall of the gear pump, through which leakage flow Q_3 passes. The length and width can be described simply by the area of the gear tooth tip, with the clearance denoted by the dimensional difference between the gear tooth tip and the internal housing surface. Again, measurable wear debris generated in this path can only conceivably come from changes in the path clearance. Thus, accounting for all three leakage passages, the amount of wear debris which is generated should be directly

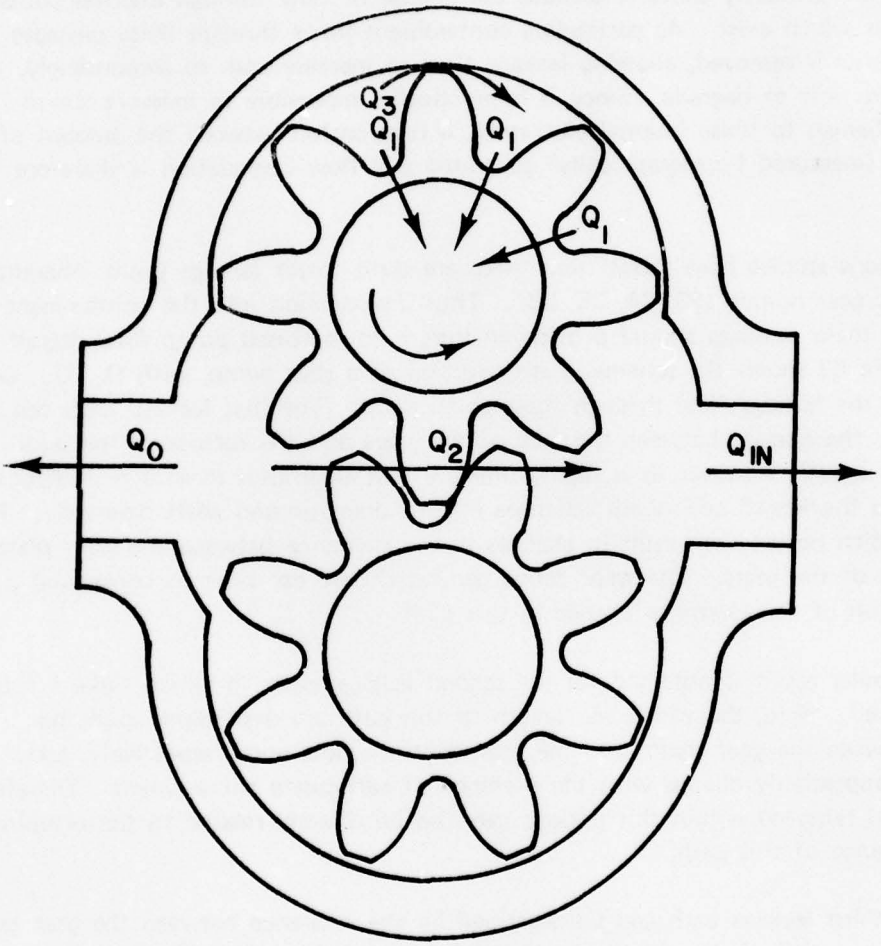

Fig. 53. Schematic Cross-Section of a Gear Pump.

proportional to the clearance change of each passage. If the total clearance for all three paths was described by an equivalent pump clearance h, then any net change in this total clearance could be described by Δh, or the change in the equivalent clearance. It is then possible to describe the volume of wear debris generated during a contaminant exposure by the following:

$$V = WL\Delta h \tag{24}$$

where: V = volume of wear debris generated
W = width of leakage path
L = length of leakage path
Δh = change in equivalent clearance of the pump

Unlike the rotary wear mechanism tests, it is impossible to measure or even control the amount of clearance in the leakage paths within the pumps. Therefore, the flow degradation resulting from each contaminant injection was recorded for correlation to corresponding Ferrographic density readings. Although not disassembled, experience suggests that the composition of the wearing parts within most gear pumps consists of steel, aluminum, and bronze or brass. However, the majority of wear will result on the gear and wear plate interface or wear of the steel and bronze or brass materials.

Test Procedure

Essentially, the test procedure used for conducting the gear pump contaminant wear tests was the same as the pump contaminant sensitivity test [23]. The major exceptions to this procedure were in the variance of the contamination level used as well as the pressure and speed at which the break-in tests were conducted. For these tests, concentration levels less than 300 mg/litre were used, and a pressure of 2500 psi at 2500 rpm was maintained during break-in.

Hydraulic gear pumps were used to evaluate the effect of various contamination levels and particle size ranges. The pumps used were all of the same lot from a particular manufacturer. Concentrations of 10, 20, 25, 75, 150, and 300 milligrams per litre and particle size ranges of 0-5, 0-10, 0-20, 0-30, 0-40, 0-50, 0-60, 0-70, and 0-80 micrometres were used as contaminant exposure levels. The speed, pressure, and temperature were maintained constant during the tests at 2000 rpm, 2000 psi, and 150°F, respectively. The general test procedure for these tests was as follows:

1. **Operate the pump at the desired conditions of speed and pressure until the temperature stabilizes at 150°F.**

2. **Accurately measure the initial flow rate of the pump and expose the required concentration of contaminant in the 0-5 micrometre size range.**

3. **Run pump with this entrained contamination level until the flow remains constant for ten minutes or until 30 minutes have elapsed. Obtain a fluid sample at the end of this period.**

4. **Valve into the system the control filters and filter oil for ten minutes. Accurately measure the flow rate of the pump.**

5. **Remove filters from the circuit and inject the appropriate concentration of contaminant at the 0-10 micrometre size range.**

6. **Repeat Steps 3, 4, and 5 until all particle size ranges (0-20, 0-30, 0-40, 0-50, 0-60, 0-70, and 0-80) have been run or until the pump is destroyed.**

A schematic of the test circuit used is shown in Fig. 54.

Test Results

The effect of the various test parameters was evaluated in terms of both flow degradation and normalized Ferrographic density (D54/ml). Since these tests were conducted in steps of particle size ranges, in order to obtain the amount of wear debris generated at each larger size (e.g., 0-30), the summation of Ferrographic density readings at the previous size ranges (i.e., (0-5) + (0-10) + (0-20)) was added to the recorded density value of the current size range. Therefore, the Ferrographic density data will be noted as Σ D54/ml.

Figures 55 and 56 show the data relating contaminant concentration to flow degradation and Ferrographic density, respectively, for particle size ranges at 2000 psi. It is quite obvious from the amount of extrapolated data in Fig. 55 that very small changes in flow result with low contaminant concentrations. This is not the case, however, with the Ferrographic density readings in Fig. 56. Here, all six concentration levels are well defined for the particle size ranges tested. As was the case with both the rotary and linear wear mechanism tests, contaminant concentration shows a greater effect than particle size on the amount of wear debris that is generated.

The following pages of photographs document the Ferrograms as they appear at the 54 mm position for various test contaminant size ranges and concentration combinations evaluated at 2000 psi. Figures 57 through 62 show the obtained wear debris

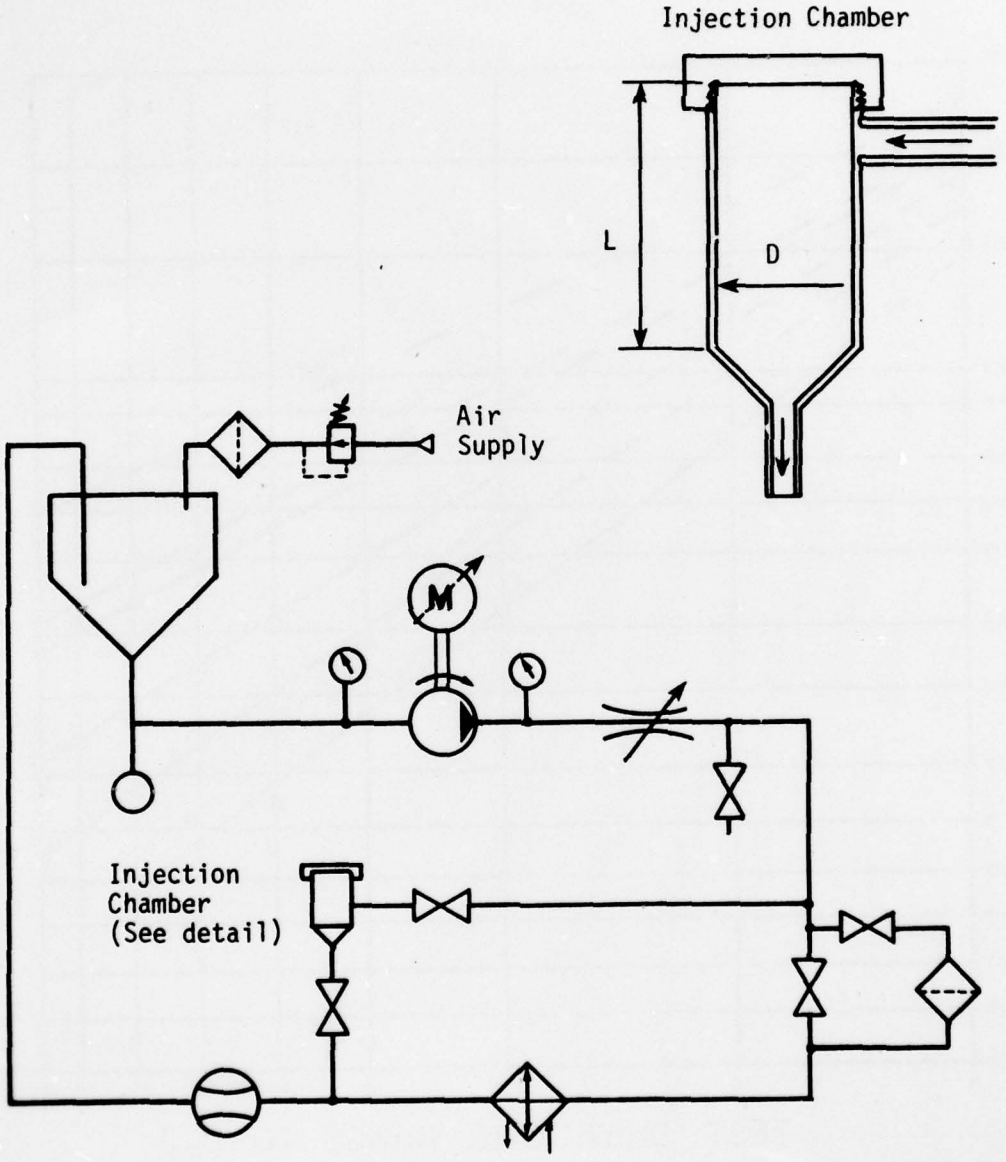

Fig. 54. Schematic of Test Circuit.

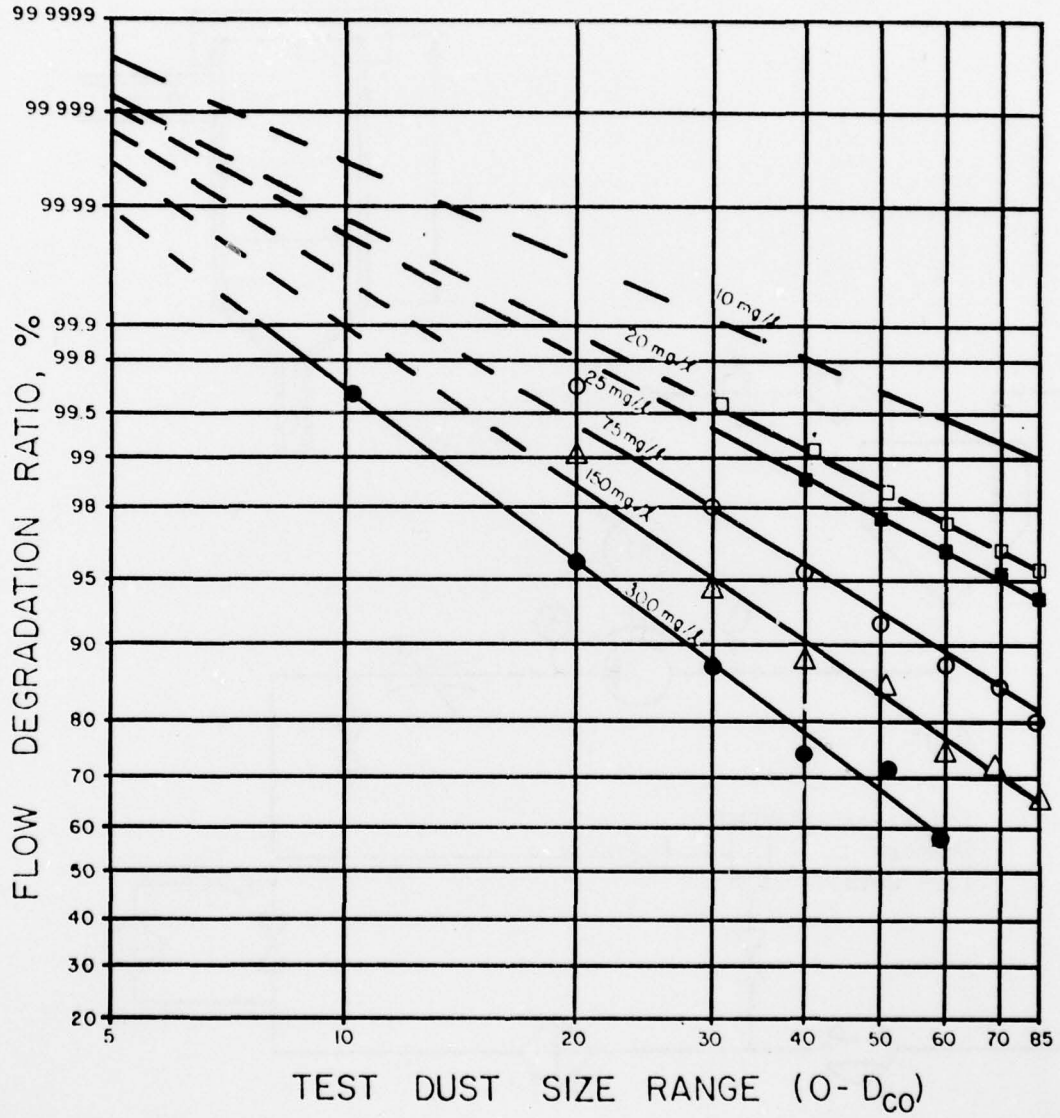

Fig. 55. Flow Degradation Ratio as a Function of Particle Size Range for Various Concentrations at 2000 psid.

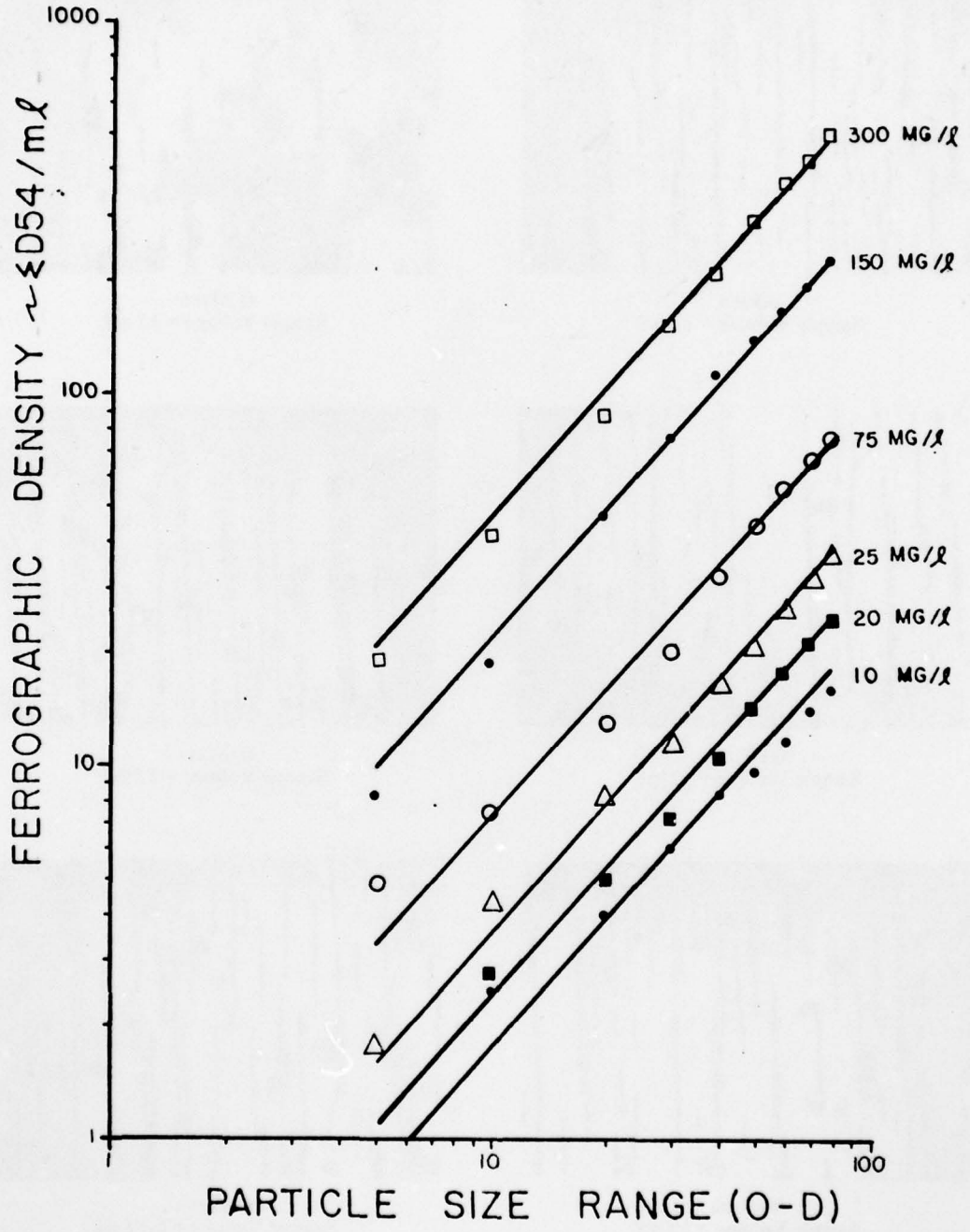

Fig. 56. Ferrographic Density as a Function of Particle Size Range for Various Concentrations at 2000 psid.

0-5 μm
Sample Volume = 12 mℓ

0-20 μm
Sample Volume = 12 mℓ

0-40 μm
Sample Volume = 12 mℓ

0-60 μm
Sample Volume = 12 mℓ

0-70 μm
Sample Volume = 12 mℓ

0-80 μm
Sample Volume = 0.12 mℓ

Fig. 57. Ferrograms of Indicated Particle Size Ranges for Pumps Run at 10 mg/ℓ of Contaminant Concentration.

0-5 μm
Sample Volume = 12 mℓ

0-20 μm
Sample Volume = 12 mℓ

0-40 μm 0-40
Sample Volume = 12 mℓ

0-60 μm
Sample Volume = 6 mℓ

0-70 μm
Sample Volume = 6 mℓ

0-80 μm
Sample Volume = 6 mℓ

Fig. 58. Ferrograms of Indicated Particle Size Ranges for Pumps Run at 20 mg/ℓ of Contaminant Concentration.

0-5 μm
Sample Volume = 6 mℓ

0-20 μm
Sample Volume = 6 mℓ

0-40 μm
Sample Volume = 6 mℓ

0-60 μm
Sample Volume = 6 mℓ

0-70 μm
Sample Volume = 6 mℓ

0-80 μm
Sample Volume = 6 mℓ

Fig. 59. Ferrograms of Indicated Particle Size Ranges for Pumps Run at 25 mg/ℓ of Contaminant Concentration.

0-5 μm
Sample Volume = 6 mℓ

0-20 μm
Sample Volume = 3 mℓ

0-40 μm
Sample Volume = 1.5 mℓ

0-60 μm
Sample Volume = 1.5 mℓ

0-70 μm
Sample Volume = 1.5 mℓ

0-80 μm
Sample Volume = 1.5 mℓ

Fig. 60. Ferrograms of Indicated Particle Size Ranges for Pumps Run at 75 mg/ℓ of Contaminant Concentration.

0-5 μm
Sample Volume = 1.5 mℓ

0-20 μm
Sample Volume = 0.6 mℓ

0-40 μm
Sample Volume = 0.6 mℓ

0-60 μm
Sample Volume = 0.6 mℓ

0-70 μm
Sample Volume = 0.6 mℓ

0-80 μm
Sample Volume = 0.6 mℓ

Fig. 61. Ferrograms of IndicatedParticle Size Ranges for Pumps Run at 150 mg/ℓ of Contaminant Concentration.

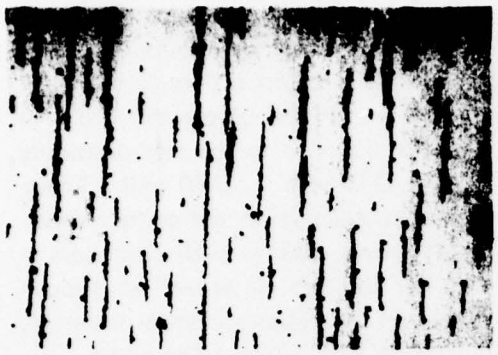

0-5 μm
Sample Volume = 12 mℓ

0-20 μm
Sample Volume = 0.6 mℓ

0-30 μm
Sample Volume = 0.6 mℓ

0-40 μm
Sample Volume = 0.3 mℓ

0-50 μm
Sample Volume = 0.12 mℓ

0-60 μm
Sample Volume = 0.12 mℓ

Fig. 62. Ferrograms of Indicated Particle Size Ranges for Pumps Run at 300 mg/ℓ of Contaminant Concentration.

at 10, 20, 25, 75, 150, and 300 mg/litre, respectively, for the various particle size exposures. These pictures cannot be directly related to the Ferrographic density curves shown in Fig. 56 due to their summation with the previously recorded density values. However, Figures 57 through 62 can be used to evaluate the effects of particle size range at the various contaminant concentrations. As was discussed in the test procedure, these particle size ranges were injected in order (0-5 μM, 0-10 μM, ..., 0-80 μM). From this fact, through analysis of the relative change in density readings as the contaminant concentration increases, a rough estimate of the internal pump leakage path clearances can be made. This can be done both visually in Figs. 57 through 62 as well as through density readings obtained for these tests. Figure 56 shows the relative change in density per change in concentration at various contaminant particle size ranges. The small changes resulting in the 0-5 and 0-10 μM exposures overall concentrations suggest that the clearances within the pumps are much larger than the contaminant. However, as the particle size range increases, the change with concentration becomes more pronounced, indicating increasing interference between the particles and the leakage path surfaces. Because of this, increases in concentration result in a substantial increase in wear debris generation. This same phenomenon can also be observed in the previous figures showing the associated Ferrograms. These observations suggest, however, that composite clearance for these pumps is probably between 5 μM and 15 μM in size.

Also evident in the Ferrograms shown in Figs. 57 through 62 are the presence of some bronze and aluminum particles. Figure 63 shows two examples of the bronze wear debris observed, and Fig. 64 indicates the presence of aluminum wear debris which was found near the exit end of the Ferrogram. Identification of the aluminum was determined by their size and location on the Ferrogram as well as their chaulky white appearance. Only a few of these particles were found, however, probably due to the magnetic properties of aluminum.

Figure 65 shows the type of wear debris observed (X1000 magnification) for selected particle size ranges of contaminant at 300 mg/litre concentration. Most noticeable is the magnitude and severity of the cutting wear particles as the contaminant size range increases. Also visible is the increase in severe wear particles (arrows) due to the larger contaminant size. The severity of this wear debris as larger contaminant size ranges are injected can be related to the increasing interference between the contaminant and leakage path clearances.

Fig. 63. Ferrograms Showing Bronze Wear Particles.

Fig. 64. Ferrograms Showing Aluminum Wear Particles.

0-20 μm

0-30 μm

0-40 μm

0-50 μm

Fig. 65. Ferrograms from Pumps at Indicated Particle Size Ranges for 300 mg/ℓ Concentration (1000X).

IX. DISCUSSION OF MECHANISM/COMPONENT RESULTS

Since the clearances within components can very rarely be measured, the component test phase could only measure flow degradation and the Ferrographic optical density of the wear debris to analyze the contaminant effects. As presented in Section VII, as long as the contaminant size remains smaller than the internal clearances, or $(h/d) >> 1$, the major type of wear debris generated will result from erosion, with the amount dependent upon the concentration. However, as the contaminant size approaches that of the internal clearances ($(h/d) \rightarrow 1$), the wear mode shifts to include abrasive wear, with the size and severity of wear debris generated dependent not only upon concentration but also the (h/d) ratios. This phenomenon did in fact occur in the test pumps, as depicted in the Ferrograms of the resulting cutting wear in Fig. 65, and was quantitatively visualized in Fig. 56 by the wear debris increase as a function of contaminant particle size and concentration. These data seem to show that clearances within the pump were between 5 μM and 15 μM in size and that (h/d) begins to approach one toward the higher particle size injection ranges.

In a qualitative inspection of the wear debris generated, both bronze and aluminum particles were identified, indicating that some relationship between the rotary wear mechanism test results for the brass/steel and aluminum/steel specimens exists and could be used to better identify the severity of wear at specific parts within the pump.

AD-A073 450 OKLAHOMA STATE UNIV STILLWATER FLUID POWER RESEARCH --ETC F/G 13/7
THE SURVIVABILITY CHARACTERISTICS OF FLUID POWER COMPONENTS IN --ETC(U)
JUN 78 N00014-75-C-1157

UNCLASSIFIED ONR-CR169-004-1 NL

2 OF 2
AD
A073450

END
DATE
FILMED
9-79
DDC

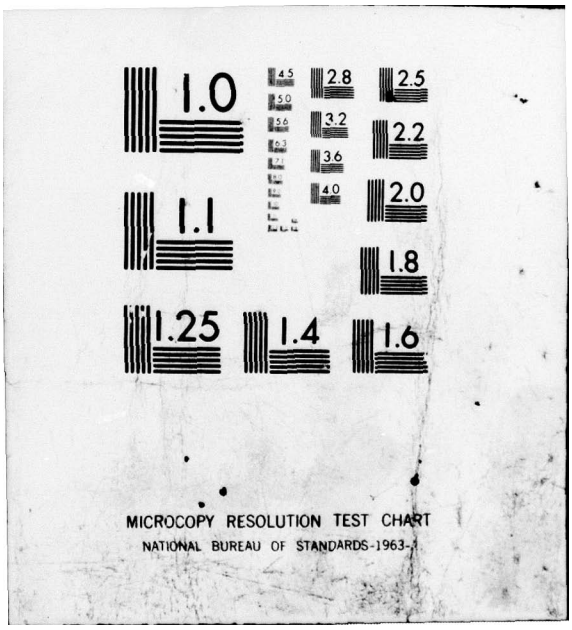
1.0
1.1
1.25
1.4
1.6
1.8
2.0
2.2
2.5
2.8
3.2
3.6
4.0
4.5
5.0
5.6
6.3
MICROCOPY RESOLUTION TEST CHART
NATIONAL BUREAU OF STANDARDS-1963-A

X. SUMMARY AND CONCLUSIONS

The basic mechanism wear tests have shown the importance of clearance size in relation to contaminant-induced wear. The rotary mechanism tests revealed the (h/d) ratio (ratio of the clearance to the largest particle diameter in a contaminant size range) is most critical in determining the type and severity of wear debris that is generated, while the linear mechanism produced similar results in addition to the *"filtering"* phenomenon, which occurs when (h/d) < 1 and alternative flow passages are present. The critical clearance at which this occurs can be identified Ferrographically.

These concepts were also verified in the component wear tests which were conducted upon hydraulic gear pumps. The test data revealed a definite increase in the magnitude and severity of wear debris as the contaminant particle size range increased and approached the clearance sizes within the test pumps. Some *"filtering"* of the contaminant particles could also be occurring as the larger particle size ranges were injected. Since it was impossible to accurately measure the existing clearances within the actual test pumps, no definite correlation of h/d could be made. However, the correlation of the pump data with the results of the mechanism testing provides an insight to the internal clearances of pumps and resulting contaminant sensitivity.

One important facet of this work was identified in analyzing pump contaminant sensitivity Ferrographically. As was shown, the conventional method of monitoring flow degradation required large amounts of contaminant (300 mg/litre) to record any appreciable degradation. The Ferrographic density values, however, were able to detect wear debris generation at contaminant concentrations as low as 10 and 20 mg/litre. Development of this information could possibly allow component contaminant sensitivity testing on a non-destructive basis.

The results of the effort have shown that the concepts developed in the rotary and linear mechanism tests provide good insight into the actual wear debris generation within a hydraulic gear pump and most likely other similar hydraulic components. As these concepts are refined, their correlation to contaminant wear will be most useful in predicting wear rates within components and eventually total hydraulic systems.

XI. REFERENCES

1. *"The Survivability Characteristics of Fluid Power Components in Contaminated Environments Annual Report,"* Contract No. N0014-75-C-1157, prepared for the Office of Naval Research by Fluid Power Research Center Personnel.

2. Seifert, W. W., and V. C. Westcott, *"A Method for the Study of Wear Particles in Lubricating Oil,"* WEAR, Vol. 21, No. 1, August 1972.

3. *"Survey of Wear Processes and the Particles from Wear by Means of a Ferrograph,"* Final Report, October 1972. Prepared by Trans-Sonics, Inc., Burlington, Massachusetts, for the Office of Naval Research, Arlington, Virginia, under Contract No. N00014-72-C-0278, NR 229-005.

4. Westcott, V. C., *"Predicting and Determining Failures by Means of Ferrography,"* Ninth Annual FAA International Maintenance Symposium, Washington, D.C., December 11-13, 1973.

5. Scott, D., W. W. Seifert, and V. C. Westcott, *"The Particles of Wear,"* SCIENTIFIC AMERICAN, Vol. 230, No. 5, May 1974, pp. 88-97.

6. Bitter, J.G.A., *"A Study of Erosion Phenomena, Part I,"* WEAR, Vol. 6, 1963, pp. 5-21.

7. Bitter, J.G.A., *"A Study of Erosion Phenomena, Part II,"* WEAR, Vol. 6, 1963, pp. 169-190.

8. Khruschov, M. M., *"Resistance of Metals of Wear By Abrasion as Related to Hardness,"* Procs. of the Conference on Lubrication and Wear, Institution of Mechanical Engineers, London, England, 1957, pp. 655-659.

9. Khruschov, M. M., and M. A. Babichev, *"Resistance to Abrasive Wear of Structurally Inhomogeneous Material,"* FRICTION AND WEAR IN MACHINERY, Vol. 12, Trans. from Russian, American Society of Mechanical Engineers, 1960, pp. 5-24.

10. Spurr, R. T., and T. P. Newcomb, *"The Friction and Wear of Materials Sliding Against Unlubricated Surfaces of Different Types and Degrees of Roughness,"* Procs. of the Conference on Lubrication and Wear, Institution of Mechanical Engineers, London, England, 1957, pp. 269-275.

11. Avient, B.W.E., J. Goddard, and H. Wilman, *"An Experimental Study of Friction and Wear During Abrasion of Metals,"* Procs., Royal Society, Vol. 258A, London, England, 1960, pp. 159-180.

12. Toporov, G. V., *"The Influence of Structure on the Abrasive Wear of Cast Iron,"* FRICTION AND WEAR IN MACHINERY, ASME Trans., Vol. 12, 1960, pp. 39-50.

13. Rabinowicz, E., L. A. Dunn, and P. G. Russel, *"The Abrasive Wear Resistance of Some Bearing Steels,"* Journal of the American Society of Lubrication Engineers, December 1961, pp. 587-593.

14. Nathan, G. K., and W.J.D. Jones, *"Influence of the Hardness of Abrasives on the Abrasive Wear of Metals,"* Procs., Institute of Mechanical Engineers, Vol. 181, Part 30, London, England, 1966-67, pp. 215-221.

15. Finkin, E. F., *"Abrasive Wear,"* Special Technical Publication 446, American Society for Testing and Materials, 1916 Race Street, Philadelphia, Pennsylvania, 1969.

16. Bensch, L. E., and E. C. Fitch, *"A New Theory for the Contaminant Sensitivity of Fluid Power Pumps,"* Paper No. 72-CC-6, Fluid Power Research Center, Stillwater, Oklahoma, 1972.

17. Fitch, E. C., *"Component Contaminant Sensitivity – A Status Report on Pumps,"* Procs. of the National Conference on Fluid Power, Vol. XXVII, Philadelphia, Pennsylvania, 1974.

18. Fitch, E. C., *"Measuring Contaminant Tolerance in Terms Compatible with Filtration Specifications – New Research Findings,"* Symposium on Contamination Control to Benefit Man and Product, Svenska Massan, Gothenburg, Sweden, April 1975.

19. Fitch, E. C., and R. K. Tessmann, *"Controlling Contaminant Wear Through Filtration,"* Third International Tribology Conference (Tribology for the Eighties), Aberdeen, Scotland, Paisley College of Technology, September 1975.

20. Seifert, W. W., and V. C. Westcott, *"Investigation of the Iron Content of Lubricating Oil Using Ferrograph and Emission Spectrometer,"* WEAR, Vol. 23, No. 2, 1973.

21. Blackburn, Reethof, and Shearer, *"Fluid Power Control,"* MIT Press, Cambridge, Massachusetts, 1960, p. 58.

22. Schlichting, H., *"Boundary Layer Theory,"* Sixth Edition, McGraw-Hill Book Co., New York, 1968.

23. *"Method of Establishing the Flow Degradation of Hydraulic Fluid Power Pumps When Exposed to Particulate Contaminant,"* T3.9.18, Milwaukee, Wisconsin, National Fluid Power Association, 1976.

24. Hunsaker, J. C., and B. G. Rightmire, *"Engineering Applications of Fluid Mechanics,"* New York, McGraw-Hill Book Company, Inc., 1947.

25. Wilson, W. E., *"Rotary-Pump Theory,"* Trans. of the ASME, Vol. 68, May 1946, pp. 371-384.

26. Wilson, W. E., *"Clearance Design in Positive-Displacement Pumps,"* Machine Design, February 1953, pp. 127-130.

DISTRIBUTION LIST

Army Materials & Mechanics Res. Ctr.
Watertown, MA 02172
C. P. Merhib 1

Admiralty Materials Laboratory
Holton Heath Poole Dorset BH16 6JU UK
Dr. G. Pocock 1

Office of Naval Research
800 N. Quincy St.
Arlington, VA 22217
LCDR H. P. Martin, Code 211 6
Dr. R. S. Miller, Code 473 1
Dr. R. Burton, Code 473 1

R&D Representative
Department of Defence
Australian High Commission Australia House
The Strand London WC2 UK
Mr. Ron A. Cummins 1

Aeronautical Research Laboratories
506 Lorimer St. Fishermen's Bend
Box 4331 PO Melbourne Victoria 3001
Australia
Mr. Max L. Atkin 1

Defence Research Establishment Pacific
Esquimalt Road Victoria British Columbia
Canada
Mr. Clint A. Waggoner 1

AFAPL/SFL
Wright Patterson AFB, OH 45433
Phillip W. Centers 1

Defense Documentation Center
Building 5, Cameron Station
Alexandria, VA 22314 12

NASA Lewis Research Center
M. S. 23-2
21000 Brookpark Road
Cleveland, OH 44135
Mr. W. J. Anderson 1

Texaco Research Center
POB 509, Beacon, N.Y. 12508
Mr. E. M. Barber 1

Mr. E. Bisson
20786 Eastwood Ave.
Fairview Parks, OH 44126 1

School of Mechanical Engineering
Upson Hall
Cornell University
Ithaca, NY 14850
Prof. J. F. Booker 1

Pratt & Whitney Aircraft
400 Main St.
EB3SW
East Hartford, CT 06108
Mr. P. F. Brown 1

Prof. W. E. Campbell
22 Ledgestone Road
Troy, NY 12180 1

Prof. of Mech. Engrg, and Astronautical
Science
Northwestern University
Evanston, IL 60201
Prof. H. S. Cheng 1

Aero Materials Department
Naval Air Development Center
Johnsville, Warminster, PA 18974
Mr. D. Minuti 1

Dr. R. S. Fain
Texaco Center
P. O. Box 509
Becon, NY 12508 1

General Electric Co., R&D Center
POB 43, Bldg. 37, Rm. 615
Schenectady, NY 12345
Mr. G. R. Fox 1

Engineering Mec. Dept., GMC-GM Research
Lab.,
12 Mile and Mound Roads
Warren, MI 48090
Mr. D. F. Hays 1

ENCLOSURE (3)

Engineering Division, Brown University
Providence, RI 02912
Prof. M. D. Hersey 1

Mr. R. L. Johnson
5304 West 62nd St.
Endina, MN 55436 1

Research Dept., Caterpillar Tractor Co.
Peoria, IL 61602
Mr. B. W. Kelley 1

Dept. of Chemical Engrg.
Pennsylvania State University
University Park, PA 16802
Prof. E. E. Klaus 1

Southwest Research Institute
8500 Culebra Road
San Antonio, TX 78284
Dr. P. M. Ku 1

The Boeing Center
POB 16858
Philadelphia, PA 19142
Mr. A. J. Lemanski, M.S. P32-09 1

Security Div., Dresser Industries
POB 24647
Dallas, TX 75224
Dr. W. E. Littmann 1

Mechanics Div., Rensselaer Polytechnic Inst.
Troy, NY 12181
Prof. J. Tichy 1

Mr. S. J. Needs, Kingsbury, Inc.
19385 Drummond Rd.
Phil., Ind. Park
Philadelphia, PA 19154 1

Mechanical Engineering Dept., MIT
Cambridge, MA 02139
Prof. Nam Suh 1

Army Research Office
POB 12211
Research Triangle Park, NC 27709
Dr. E. A. Saibel 1

Mechanical Eng. Dept., University of Wisconsin
1513 University Avenue
Madison, WI 53706
Prof. A. Seireg 1

SKF Technology Service
1100 First Ave.
King of Prussia, PA 19406
Mr. L. B. Sibley 1

Mechanical Technology, Inc.
968 Albany Shaker Rd.
Latham, NY 12110
Dr. D. F. Wilcock 1

Mechanical Eng. Dept.
University of Massachusetts
Amherst, MA 01002
Prof. W. R. D. Wilson 1

Mechanical Engineering Dept.
Georgia Institute of Technology
Atlanta, GA 30332
Prof. W. O. Winer 1

U. S. Naval Research Laboratories
Washington, DC 20375
Mr. R. C. Bowers 1

Office of Technology Assessment
Congress of the United States
Washington, DC 20510
Mr. M. B. Peterson 1

Air Force Aero Propulsion Laboratory
Wright Patterson Air Force Base, OH 45433
Mr. H. F. Jones 1

MS 23-2, NASA-Lewis Research Center
21000 Brookpark Rd.
Cleveland, OH 44135
Mr. L. P. Ludwig 1

Air Force Materials Lab.
Wright Patterson Air Force Base
Dayton, OH 45433
Mr. F. Brooks 1

Mobil Research & Development Corp.
Box 1025 Princeton, NJ 08540
C. N. Rowe 1

NASA-Lewis Research Center
21000 Brookpark Road
Cleveland, OH 44135
E. V. Zaretsky 1

Commander
Naval Air Systems Command
Washington, DC 20361
Code 340E (Mr. B. Poppert) 1

Naval Air Engineering Center
Ground Support Equipment Department
Lakehurst, NJ 08733
Code 92724 (P. Senholzi) 1

National Bureau of Standards
Department of Commerce
Washington, DC 20234
Dr. W. Ruff 1

Imperial College of Science and
Technology
Dept. of Mechanical Engineering
Exhibition Road
London, England SW7
Prof. P. Macpherson 1

Commander
Naval Sea Systems Command
Code 0484G
Washington, DC 20362
Mr. Tarte 1

Foxboro Analytical
Burlington Center
78 Blanchard Road
P. O. Box 435
Burlington, MA 01803 1

Mechanical Engineering Department
Michigan Technological University
Houghton, MI 49931
Dr. John Johnson 1